Pergamon

Geochimica et Cosmochimica Acta, Vol. 66, No. 4, pp. 661–682, 2002

0016-7037/−1898 $22.00 + .00

PII S0016-7037(01)00802-X

Volatilization kinetics of silicon carbide in reducing gases: An experimental study with applications to the survival of presolar grains in the solar nebula

R. A. MENDYBAEV,[1,2]* J. R. BECKETT,[2] L. GROSSMAN,[1,3] E. STOLPER,[2] R. F. COOPER,[4] and J. P. BRADLEY[5,6]

[1]Department of the Geophysical Sciences, University of Chicago, Chicago, IL 60637, USA
[2]Division of Geological and Planetary Sciences, California Institute of Technology, Pasadena, CA 91125, USA
[3]Enrico Fermi Institute, University of Chicago, Chicago, IL 60637, USA
[4]Department of Materials Science and Engineering, University of Wisconsin, Madison, WI 53706, USA
[5]MVA Inc., Norcross, GA 30093, USA
[6]School of Materials Science and Engineering, Georgia Institute of Technology, Atlanta, GA 30332, USA

(*Received April* 26, 2001; *accepted in revised form August* 21, 2001)

Abstract—The volatilization kinetics of single crystal α-SiC, polycrystalline β-SiC, and SiO_2 (cristobalite or glass) were determined in H_2-CO_2, CO-CO_2, and H_2-CO-CO_2 gas mixtures at oxygen fugacities between 1 log unit above and 10 log units below the iron–wüstite (IW) buffer and temperatures in the range 1151 to 1501°C. Detailed sets of experiments on SiC were conducted at 2.8 and 6.0 log units below IW (IW-2.8 and IW-6.0) at a variety of temperatures, and at 1300°C at a variety of oxygen fugacities. Transmission electron microscopic and Rutherford backscattering spectroscopic characterization of run products shows that the surface of SiC exposed to IW-2.8 is characterized by a thin (<1 μm thick), continuous layer of cristobalite. SiC exposed to IW-6.0 lacks such a layer (or its thickness is <0.01 μm), although some SiO_2 was found within pits and along incised grain boundaries.

In H_2-CO_2 gas mixtures above ~IW-3, the similarity of the SiC volatilization rate and of its dependence on temperature and fO_2 to that for SiO_2 suggests that SiC volatilization is controlled by volatilization of a SiO_2 layer that forms on the surface of the SiC. With decreasing log fO_2 from ~IW-3 to ~IW-6, the SiC volatilization rate is constant at constant temperature, whereas that for SiO_2 increases. The independence of the SiC volatilization rate from the gas composition under these conditions suggests that the rate-controlling step is a solid–solid reaction at the internal SiC/SiO_2 interface. For gas compositions more reducing than ~IW-6, the SiC volatilization rate increases with decreasing fO_2, with both bare SiC surfaces and perhaps silica residing in pits and along incised grain boundaries contributing to the overall reaction rate.

If the volatilization mechanism and reaction rate in the solar nebula were the same as in our H_2-CO_2 experiments at IW-6.0, then estimated lifetimes of 1-μm-diameter presolar SiC grains range from several thousand years at ~900°C, to ~1 yr at 1100°C, ~1 d at 1300°C, and ~1 h at 1400°C. The corresponding lifetimes for 10-μm SiC grains would be an order of magnitude longer. If the supply of oxidants to surfaces of presolar SiC grains were rate limiting—for example, at $T > 1100$°C for $P^{tot} = 10^{-6}$ atm and sticking coefficient = 0.01, then the calculated lifetimes would be about 10 yr for 10-μm-diameter grains, essentially independent of temperature. The results thus imply that presolar SiC grains would survive short heating events associated with formation of chondrules (minutes) and calcium-, aluminum-rich inclusions (days), but would have been destroyed by exposure to hot (≥900°C) nebular gases in less than several thousand years unless they were coated with minerals inert to reaction with a nebular gas.

1. INTRODUCTION

The mineral moissanite, naturally occurring hexagonal silicon carbide (α-SiC), and β-SiC, the cubic form, are occasionally reported in terrestrial rocks (Bauer et al., 1963; Marshintsev et al., 1982; Leung, 1990; Filippidis, 1993), although these descriptions are often met with open skepticism because α-SiC is an extensively used abrasive (e.g., Milton and Vitaliano, 1984). Moissanite may also occur in primitive chondritic meteorites, but as with terrestrial samples, it is difficult to dismiss laboratory contamination because the isotopic compositions are consistent with the crystals being terrestrial contaminants (Virag et al., 1992). On the other hand, natural β-SiC is unambiguously present in these same meteorites, and it assumes great importance because it is the carrier of Ne-E (essentially pure ^{22}Ne), Xe-S, and Kr-S, which display the isotopic signatures of *s*-process nucleosynthesis, and large isotopic anomalies in a variety of other elements, including C, N, Si, Al, Mg, Ti, Zr, and Mo (Bernatowicz et al., 1987; Zinner et al., 1987; Tang and Anders, 1988; Anders and Zinner, 1993; Hoppe et al., 1994; Lewis et al., 1994; Hoppe and Ott, 1997; Huss et al., 1997; Nicolussi et al., 1997, 1998). The chemical and isotopic characteristics of meteoritic β-SiC indicate that these grains probably formed as stable phases in the C-rich environments (C/O greater than ~1) of asymptotic giant branch (AGB) stars and supernovae (e.g., Amari and Zinner, 1997; Hoppe and Ott, 1997). Equilibrium calculations show, however, that SiC is thermodynamically unstable over all temperatures in a gas of solar composition (Lattimer and Grossman, 1978; Larimer and Bartholomay, 1979). Hence, it is expected that the injection of presolar SiC grains into the solar nebula would result in volatilization (e.g., Fegley, 1988) during energetic processes such as passage through the accretion shock front bounding the nebula (Wood and Morfill, 1988; Ruzmaikina and Ip, 1994;

* Author to whom correspondence should be addressed (ramendyb@midway.uchicago.edu).

Cassen and Chick, 1997) or high-temperature events within the nebula that caused condensation of refractory inclusions and melting of chondrules (Grossman, 1972; Davis and MacPherson, 1996; Hewins and Connolly, 1996). The fact that some presolar SiC grains survived these processes and accreted into the same meteorites as high-temperature refractory inclusions and chondrules suggests that chemical reactions leading to the destruction of these grains were kinetically inhibited. By considering the conditions under which SiC grains could have survived transport into the primitive solar nebula and eventual incorporation into primitive meteorites, it may be possible to constrain the timing of arrival of interstellar grains relative to the attainment of high nebular temperatures and the duration of high temperatures in certain nebular regions.

Although oxidation of SiC has been studied intensively because of its commercial significance, most of the data refer to experiments conducted in oxygen or air (dry or with some amount of water vapor), often diluted with noble gases (see reviews of Jacobson, 1993; Narushima et al., 1997). Studies that use gases of interest to meteoritic systems are limited to H_2-H_2O (Kim, 1987; Kim and Readey, 1989; Jacobson et al., 1990), CO-CO_2 (Narushima et al., 1993, 1994), and N_2-H_2-CO (Butt et al., 1992). Classically, the oxidation of SiC is viewed as occurring in one of two distinct regimes: active oxidation, by which SiC loses weight as a function of time, and passive oxidation, which is characterized by continuous weight gain. It is well established (Jacobson, 1993; Narushima et al., 1997) that passive oxidation reflects the formation and growth of a layer of silica on the surface of SiC through reactions such as

$$SiC_{(s)} + 3/2O_{2(g)} \rightarrow SiO_{2(s)} + CO_{(g)}, \quad (1)$$

$$SiC_{(s)} + 3H_2O_{(g)} \rightarrow SiO_{2(s)} + CO_{(g)} + 3H_{2(g)}, \quad (2)$$

and

$$SiC_{(s)} + 3CO_{2(g)} \rightarrow SiO_{2(s)} + 4CO_{(g)}. \quad (3)$$

Experimental data for passive oxidation of SiC are usually described in terms of parabolic or linear–parabolic kinetics—that is, weight gain is a parabolic or linear–parabolic function of time (e.g., Ervin, 1958; Jorgensen et al., 1959; Gulbransen and Jansson, 1972; Costello and Tressler, 1981; Jacobson, 1993; Narushima et al., 1997). In contrast, weight loss in the classical active regime is typically a linear function of time (e.g., Kim, 1987; Narushima et al., 1997) and may occur through direct vaporization of SiC to gaseous products via reactions such as

$$SiC_{(s)} + O_{2(g)} \rightarrow SiO_{(g)} + CO_{(g)}, \quad (4)$$

$$SiC_{(s)} + 2H_2O_{(g)} \rightarrow SiO_{(g)} + CO_{(g)} + 2H_{2(g)}, \quad (5)$$

and

$$SiC_{(s)} + 2CO_{2(g)} \rightarrow SiO_{(g)} + 3CO_{(g)}, \quad (6)$$

which we refer to as the "true active oxidation regime," or by formation and volatilization of a steady-state silica layer that partially or completely covers the surface of SiC (e.g., Rosner and Allendorf, 1970; Antill and Warburton, 1971; Kim and Readey, 1989; Schneider et al., 1998), which, following Opila and Jacobson (1995), we refer to as the "coupled oxidation and volatilization regime." As fO_2 is increased from very low levels at constant temperature, the mode of SiC oxidation changes from true active to coupled oxidation–volatilization to passive regimes (Opila and Jacobson, 1995). A maximum in the SiC volatilization rate as a function of fO_2 within the classical active regime (e.g., Rosner and Allendorf, 1970; Narushima et al., 1991; Schneider et al., 1998) may be related to the transition between true active oxidation of bare SiC and volatilization of a steady-state silica layer on SiC. The experimentally determined fO_2 for this maximum as well as for the classical active-to-passive transition (i.e., weight loss vs. weight gain) is a function of temperature, total pressure, gas composition, and flow rate (Gulbransen et al., 1966; Rosner and Allendorf, 1970; Kim, 1987; Kim and Readey, 1989; Narushima et al., 1991, 1994).

The focus of our work is to provide estimates of maximum timescales for survival of presolar grains in nebular environments. In this article, we report the results of experimentally determined kinetics of SiC volatilization as a function of temperature, gas composition, and flow rate in H_2-CO_2, CO-CO_2, and H_2-CO-CO_2 gas mixtures. At low oxygen fugacities, the H_2-CO_2 and H_2-CO-CO_2 gas mixtures are much closer to a gas of solar composition than are the H_2-H_2O or CO-CO_2 mixtures used by previous workers. Because silica appears to play an important role in SiC volatilization over much of the range in redox conditions considered in this study, we also performed experiments on the volatilization rate of silica (cristobalite or glass). Finally, we discuss possible volatilization mechanisms of SiC within the range of oxygen fugacities from 1 to 10 log units below that corresponding to the iron–wüstite (IW) buffer (i.e., IW-1 to IW-10), which is appropriate for solar nebular environments (nominally ~IW-6 with possible variations of three or four log units, Rubin et al., 1988), and use these results to constrain the lifetimes of interstellar grains of SiC in the inner solar nebula.

2. EXPERIMENTAL TECHNIQUES

2.1. Starting Materials

Starting materials for oxidation experiments on silicon carbide were produced from dark gray opaque fragments (~2.5 × 2.5 × 0.5 cm) of single crystal α-SiC synthesized by the Acheson process (>99.99% SiC; Elektroschmelzwerk Delfzijl) and plates (~4 × 3 × 0.4 cm) of polycrystalline chemically vapor deposited (CVD) β-SiC with crystallites of ~5 to 10 μm (>99.999% SiC; Morton International). As starting materials for silica volatilization experiments, we used wafers cut from optically clear fused quartz disks, ~1.5 cm in diameter and 2 mm thick (>99.9%, General Electric Co.). Purities of the starting materials are given as provided by manufacturers. Our scanning electron microscopic (SEM) analyses of single crystal α-SiC showed an Fe content of less than 100 ppm. Crystal structures of the SiC samples were confirmed by X-ray diffraction (XRD) analysis, and SEM examination revealed no voids, microcracks, or porosity. The densities of both α- and β-SiC as measured with a Berman balance and calculated from the size and weight of polished wafers was 3.2 g/cm^3, which is equal to the theoretical density.

Wafers of SiC and SiO_2 for experiments were prepared by cutting as-received material with an ISOMET (Buehler) low-speed diamond saw. The wafers had typical dimensions of ~6 × 2.5 × 0.3 mm (determined with a micrometer with a precision of 1 μm), yielding an initial surface area of 35 to 55 mm^2 and a weight of 10 to 25 mg. Uncertainties (1σ) in the initial weights of individual wafers used in the experiments were usually less than 0.001 mg. Although all surfaces were polished, the wafers were slightly nonuniform in thickness, re-

sulting in relatively large uncertainties in surface area (usually <2 mm^2). Each wafer was polished successively by 60-, 30-, 10-, 5-, and 1-μm diamond powder with thorough ultrasonic cleaning in acetone, isopropanol, ethanol, and deionized water. Resulting wafers were translucent with a deep blue (α-SiC) or dark yellow (β-SiC) color. Samples were dried in a vacuum at 120°C for at least 1 d and stored in a desiccator before use.

Most of our volatilization experiments were conducted in H_2-CO_2 gas mixtures; a few experiments were run in CO-CO_2 or H_2-CO-CO_2. Nitrogen was used as a purge gas; it was also used as a relatively nonreactive carrier during sample insertion into the furnace before the beginning of each experiment. Gas mixtures of various compositions were prepared from tanks of >99.95% pure H_2, CO_2 and N_2 (all from Air Liquide) and 99.5% pure CO (Matheson Gas Products) with a gas-mixing apparatus.

2.2. Analytical Methods

Surfaces and cross sections of the starting materials and experimental run products were examined optically by XRD, a JEOL JSM-35 scanning electron microscope, a 200-keV JEOL 2010 analytical transmission electron microscope, and Rutherford backscattering spectroscopy (RBS). Samples for transmission electron microscopic (TEM) analysis were prepared by fabrication of multilayered cross sections of SiC wafer fragments, polishing with successively finer ($15 \rightarrow 3$ μm) diamond pastes, dimple grinding, and finally ion-milling to electron transparency in a liquid-nitrogen–cooled stage with 2 to 5 keV Ar^+ (Bravman and Sinclair, 1984). RBS is a nondestructive, standardless method of composition profiling that does not require any special sample preparation. The basic idea of this technique is that a high-energy α particle ($^4He^+$) elastically striking an atom on the free surface of a specimen will backscatter at a particular energy, but if the α particle penetrates into the sample, it will lose energy through inelastic ionization reactions. The energy loss due to collision with component atomic nuclei is virtually independent of bonding environment but correlates with composition (Chu et al., 1978). Because ion-stopping and ion-backscattering cross sections are well understood for energies above ~0.4 MeV, one can use spectral simulations (e.g., Doolittle, 1985) to obtain chemical information as a function of depth. RBS has a spatial (depth) resolution of ~0.01 μm and can be used to obtain composition profiles to a depth of 2 to 3 μm. We employed α particles accelerated to an initial kinetic energy of 2 MeV. Details of instrumentation and spectral simulation procedures are given in Cooper et al. (1996).

2.3. Furnace Configuration and Experimental Protocol

Experiments were conducted in a vertical 1 atm Deltech furnace with $MoSi_2$ heating elements and a Eurotherm 812 controller/programmer (Fig. 1). The temperature in the furnace hot spot was in the range 1151 to 1501°C as measured by a Pt/Pt10Rh (type S) thermocouple located inside the oxygen sensor and calibrated against the melting point of gold. Reported temperatures are believed accurate to within ±3°C. Gas mixtures were introduced into the top of a 3.2-cm-diameter alumina tube (99.8% Al_2O_3; Vesuvius McDanel) and exhausted from its bottom. Relative volumes of gases in the flowing gas mixtures (e.g., 96.4%H_2 + 3.6%CO_2, or 98.9%CO + 1.1%CO_2 at IW-2.8; 99.9%H_2 + 0.1%CO_2, or 99.97%CO + 0.03%CO_2 at IW-6.0) and their flow rates (from 0.3 to 1.6 cm/s) were determined by use of the floating soap bubble technique of Nafziger et al. (1971). The oxygen fugacity for experiments was in the range IW+1 to IW-10 as determined by an yttria-doped zirconia (YSZ) solid electrolyte oxygen sensor (SIRO2; Ceramic Oxide Fabricators). Corrections for non-Nernstian behavior of the electrolyte were made according to procedures described in Mendybaev et al. (1998). The uncertainty in log fO_2 ranges from less than ±0.05 in the vicinity of IW to ~ ±0.2 at IW-6 (solar gas) and to approximately ±0.5 at log fO_2 = IW-9, where the errors cited here and below refer to one standard deviation of the mean. Because of the high temperatures of our experiments, the mixed gases achieved equilibrium without the aid of a catalyst (Beckett and Mendybaev, 1997). In the presence of vaporizing SiC or SiO_2, the vapor pressure of SiO over the wafers can be high enough under reducing conditions to form Pt-Si or Pt-Rh-Si alloys with low melting temperatures. The tip of the oxygen sensor was therefore placed approximately 1 cm above the sample to avoid damage to the external electrode of the oxygen sensor and its electrical lead (Pt or Pt-Rh). Because the hot spot over which the temperature is constant within 1°C in our apparatus is ~3 cm in height, this artifice introduced no significant offsets between measured temperatures or oxygen fugacities and those experienced by the samples.

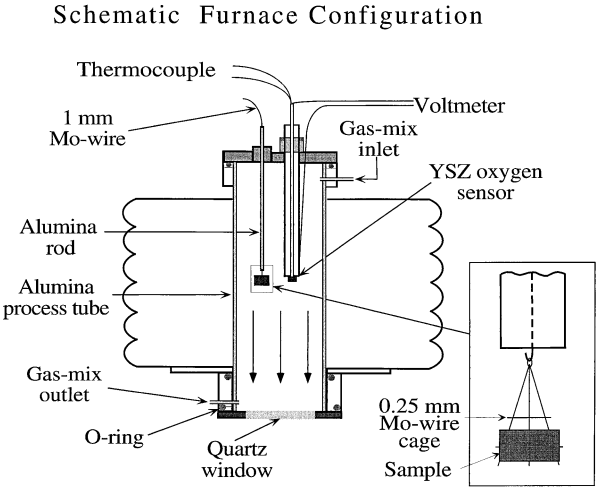

Fig. 1. Schematic configuration of furnace used in experiments below IW. Vertical arrows inside the process tube indicate the direction of gas flow. The configuration for experiments conducted above IW was identical except that an Ir-wire cage was suspended from Pt wire.

The assembly for experiments at oxygen fugacities below IW consisted of a YSZ oxygen sensor and an alumina rod containing a 1-mm-diameter Mo wire hook from which the sample wafer, which was held in a Mo-wire cage, was suspended. Mo was chosen because it is thermodynamically stable at oxygen fugacities below IW, has a low vapor pressure under the conditions of our experiments, and is chemically inert with respect to SiC and SiO_2. The wire cage, shown as an inset in Figure 1, was constructed from three 0.25-mm-diameter, 2- to 3-cm-long Mo wires. At one end, the wires were twisted together and bent to form a hook that we used to suspend the cage from the Mo-wire hook extending from the alumina rod. At the other end, the wires were flared out such that the outer two wires were a maximum of ~0.8 cm apart, and then each of the wires was bent into a hook to be used to help hold the wafer (i.e., the wafer was oriented with the large faces parallel to gas flow). One or two lengths of Mo wire were also welded across the set of flared wires to generate a rigid structure. In experiments at oxygen fugacities above IW, the Mo wire was replaced by 0.5-mm Pt wire, and the cage was made of Ir wire.

To begin an experiment, the hot spot temperature of the furnace was adjusted to 1000°C and the alumina tube flushed with N_2. A ready-to-run wafer of SiC or SiO_2 was taken out of the desiccator, weighed several times, and placed in the cage attached to the sample assembly. The sample assembly was then inserted into the furnace such that the oxygen sensor was ~1 cm above the hot spot but the Mo- or Ir-wire cage containing the SiC or SiO_2 wafer was ~3 to 4 cm below the top of the furnace in a cool (50 to 60°C) zone. The furnace temperature was increased to that of the experiment, the N_2 shut off, and the desired gas mixture introduced. Once the temperature and oxygen fugacity stabilized at the run conditions, the cage containing the sample wafer was quickly (within a few seconds) moved to the hot spot by lowering the alumina rod from which it was suspended (see Fig. 1). It was exposed to the gas for a predetermined length of time, then quickly removed from the hot spot by pulling the sample up into the cool region of the furnace. At this point, the mixed gas of the experiment was turned off and N_2 turned on to flush the furnace. Once the oxygen sensor indicated an oxygen fugacity corresponding to that of the commercial grade N_2, the sample was removed from the furnace and weighed several times. Sample weights were measured with a CAHN C-30 Microbalance (CAHN Instruments) to a precision of ±0.5 μg. The balance was calibrated before each measurement with class 1 standard weights.

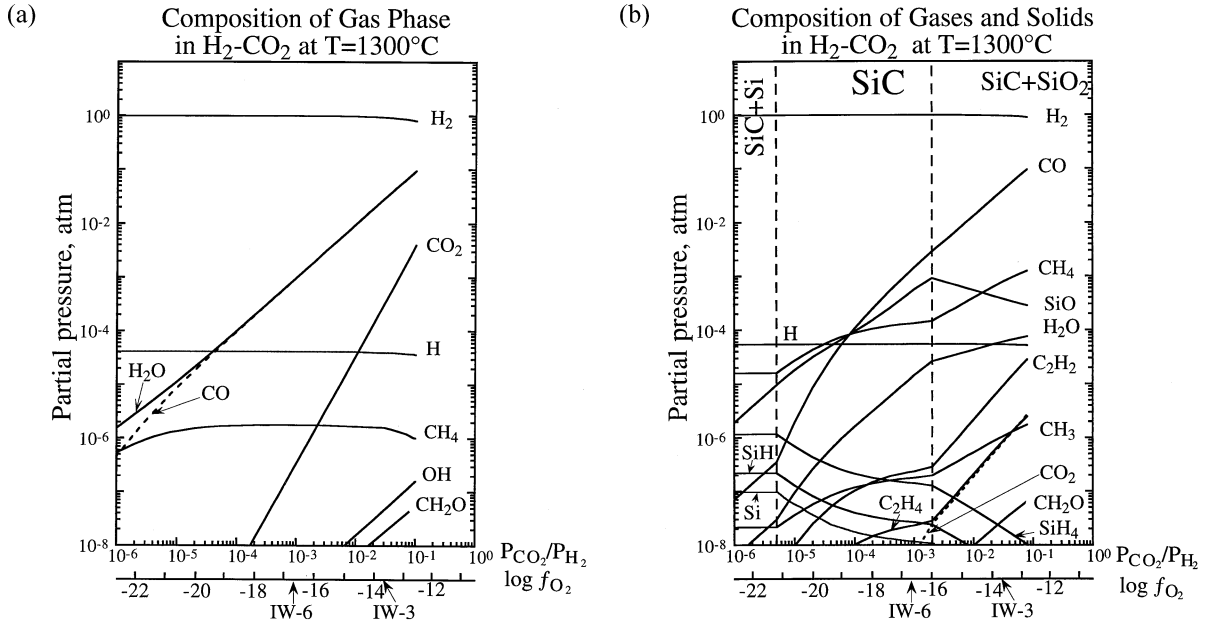

Fig. 2. Equilibrium speciation at 1300°C as a function of initial CO_2/H_2 ratio and log fO_2 of H_2-CO_2 gas mixtures. Thermodynamic data were taken from Chase et al. (1985) except for those for C_2H_2 and β-SiC, which were taken from Barin (1989). Positions of log fO_2 = IW-3.0 and IW-6.0 are shown (log $fO_2 = -10.73$ at IW and 1300°C). (a) Composition of gas phase in H_2-CO_2 at T = 1300°C for the pure gas mixtures. (b) Composition of gases and solids in H_2-CO_2 at T = 1300°C for systems containing equal moles of SiC and $H_2 + CO_2$ at P^{tot} = 1 atm. Vertical dashed lines show boundaries between stability fields of solids.

The above process was repeated as often as required to obtain a significant weight change (at least several micrograms and generally much more) in the SiC or SiO_2 wafers and to determine the dependence of the weight change on time. Run durations varied from several hours to several weeks, depending on the temperature and the composition of the experimental gas mixture. Several experiments were usually performed on each wafer, the history of which can be traced through entries in the data tables. Reaction rates were obtained by plotting weight change vs. time, and error propagation was performed by least-square methods.

3. RESULTS

3.1. Thermodynamics of SiC Volatilization

The equilibrium speciation for pure H_2-CO_2 gas mixtures at 1300°C was calculated by the computer program of Yoneda and Grossman (1995), which is based on the Gibbs energy minimization method, and plotted as a function of initial CO_2/H_2 ratio and fO_2 in Figure 2a. It is seen that H_2 is the dominant species in H_2-CO_2 gas mixtures at 1300°C, and its partial pressure is almost independent of fO_2. The major oxygen-bearing species are H_2O, CO, and CO_2, and their equilibrium partial pressures increase by several orders of magnitude as the gas becomes more oxidizing. In contrast, partial pressures of major species in a gas of constant bulk composition remain nearly the same within the whole range of temperatures used in our experiments.

To see the effect of SiC volatilization on the composition of the experimental gas mixtures, the equilibrium distribution of elements between gaseous species and solid phases was calculated at 1300°C for systems whose bulk compositions consist of equal numbers of moles of SiC and $H_2 + CO_2$. Such a large solid/gas ratio guarantees the presence of the solid phases, and calculated partial pressures represent the equilibrium composition of the vapor above the solid. Results are shown in Figure 2b, again as a function of initial CO_2/H_2 ratio and fO_2. A diagram of this type can be a useful guide for identifying likely reactions between gases and solids as the gas phase varies systematically in composition. For example, under extremely reducing conditions (log $fO_2 < -20.9$ or $<$ IW-10.5), not covered by our experiments, Figure 2b shows that SiC and solid or liquid silicon are stable, and that partial pressures of silicon-bearing species are very low. Under more oxidizing conditions ($-20.9 <$ log $fO_2 < -15.9$), the only solid phase is SiC, and P_{SiO} increases as the gas becomes more oxidizing. In this range of fO_2, active oxidation would be expected, and because the partial pressures of H_2O and CO_2 are considerably higher in the gas mixtures (Fig. 2a) than for gases equilibrated with SiC (Fig. 2b) at the same fO_2, the responsible reactant is expected to be H_2O (reaction 5) or perhaps CO_2 (reaction 6). As the gas becomes even more oxidizing (log $fO_2 > -15.9$), passive oxidation of SiC via reactions 2 and 3 would be expected, resulting in the formation of silica. It should be noted that the precise position of the transition between active and passive oxidation cannot be read directly from Figure 2b. Other factors, such as mass transport through the gaseous boundary layer around SiC, need to be considered.

3.2. Kinetics of SiC Volatilization

3.2.1. Selection of Experimental Conditions for Oxidation of SiC

To establish a baseline for the behavior of SiC in mixed gases, we first conducted a set of reconnaissance experiments

Table 1. Initial weight change of fresh SiC wafers in H_2-CO_2 as a function of temperature and fO_2.

T (°C)	log fO_2	Run duration (h)	Weight change[a]
1195	−14.68	12	No change
1196	−15.09	15	No change
1196	−16.43	45	Loss
1197	−15.65	9.5	Loss
1197	−16.41	9.5	Loss
1197	−17.90	9	Loss
1201	−13.80	30	Gain
1203	−14.70	60	Gain
1229	−17.50	12	Loss
1295	−12.44	8	No change
1295	−12.88	3	Loss
1300	−9.70	3	Gain
1300	−10.70	1	Gain
1300	−11.70	11	Gain
1300	−12.70	1	No change
1343	−11.55	1.5	No change
1343	−12.37	2.5	Loss
1390	−15.70	0.5	Loss
1391	−12.49	2	Loss
1392	−11.24	1.5	No change
1392	−11.46	1.5	Loss
1392	−11.89	2	Loss
1393	−12.86	2	Loss
1402	−12.50	1	Loss
1437	−9.65	0.5	Gain

[a] "Gain" or "loss" indicates a change in weight exceeding 0.001 mg over the course of the experiment. "No change" indicates that the weight change was less than 0.001 mg.

that used freshly polished SiC wafers. These are wafers that were never used in previous experiments. Although it is possible that a very thin layer of silica exists on their surfaces, we were unable to detect it by TEM. Results are given in Table 1. For most of these experiments, data were collected only for a time sufficient to determine whether weight was initially gained or lost. Results for all experiments of this type are summarized in Figure 3 in which the direction of weight change is shown in terms of T-fO_2 for H_2-CO_2 gas mixtures. Below the thick, solid curve in Figure 3, freshly polished SiC wafers lose weight instantaneously within the error of our measurements. This curve thus provides a convenient demarcation for the oxygen fugacities below which a silica layer either does not form on the surface of a fresh SiC wafer or is so thin that linear weight loss prevails over all experimental timescales. It is important to recognize that the curve does not represent the boundary between classical active (weight loss) and passive (weight gain) oxidation regimes of SiC in H_2-CO_2 gas mixtures. Classical passive oxidation, in which weight gain persists beyond an initial short time period, occurs under conditions more oxidizing than the curve shown in Figure 3 (e.g., Schneider et al., 1998). Furthermore, transient weight gains are expected at fO_2s even lower than the curve shown in Figure 3, as were seen in short duration experiments in which sample weight was monitored continuously in other gas mixtures (e.g., Jacobson et al., 1990; Narushima et al., 1997).

To elucidate further the nature of the different regimes outlined in Figure 3, we conducted a few, more detailed experiments, again on freshly polished SiC wafers, representative

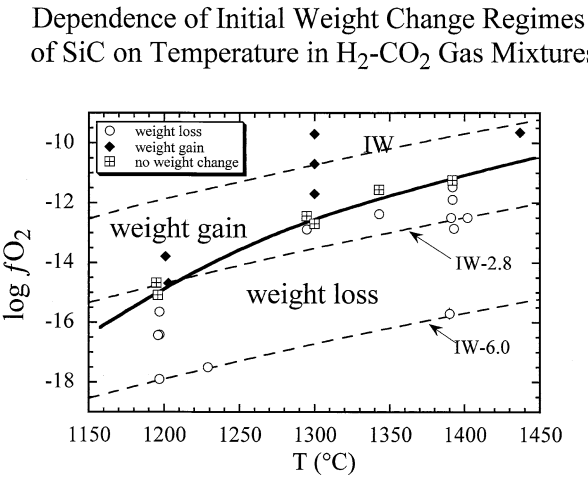

Fig. 3. Dependence of initial weight change regimes of SiC on temperature in H_2-CO_2 gas mixtures. Closed symbols indicate samples that initially gained weight; open symbols indicate those that lost weight; crossed symbols indicate those that changed weight by <1 μg over the course of the experiment. The thick, solid curve separates fields of initial weight gain and weight loss regimes. For reference, the positions of the IW buffer, IW-2.8 and IW-6.0 are shown as thin, dashed curves.

results for which are shown in Figure 4. Depending on experimental conditions, one of three different weight change patterns was observed. Curves a and b in Figure 4 show weight gain and weight loss with time, corresponding to classical passive and active oxidation, respectively. Curve c displays an initial increase in weight after which the weight loss is linear with time, a phenomenon known as paralinear behavior (Opila and Jacobson, 1995; Opila and Hann, 1997). These workers demonstrated that after an initial formation period, the thick-

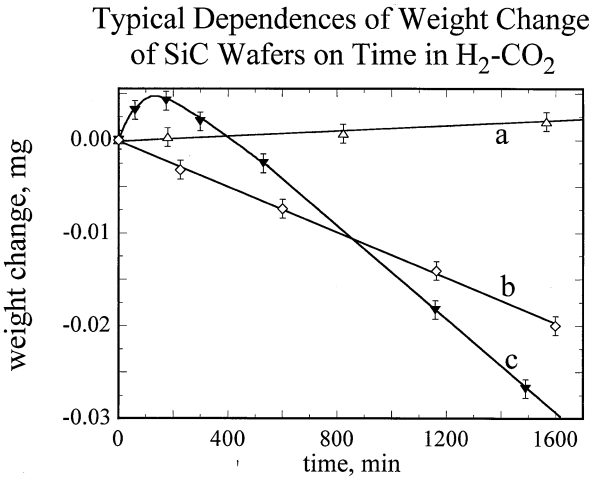

Fig. 4. Typical regimes of SiC oxidation in H_2-CO_2 gas mixtures. (a) Classical passive (T = 1203°C, log fO_2 = IW-2). (b) Classical active (T = 1198°C, log fO_2 = IW-6). (c) Coupled oxidation and volatilization (T = 1300°C, log fO_2 = IW+1). A fresh SiC wafer was used in each run. Unless otherwise stated, error bars in this and succeeding figures refer to one standard deviation of the mean. Error bars are shown where they are larger than the symbol size.

ness of the silica layer (up to several microns in oxidizing gases) remains essentially constant as volatilization proceeds. The initial weight gain for experiments with curves similar in appearance to that of curve c, typically 5 to 10 μg, is equivalent to the weight that would be gained in forming a ~0.05- to 0.1-μm-thick silica layer over the entire surface of the wafer. We show below that silica layers are in fact formed in many experiments, although our microbalance precision of ± 0.5 μg makes detection of such layers ≤ 0.005 μm thick impossible by weighing only. The duration of an initial stage of weight gain is very sensitive to the experimental conditions, generally decreasing as temperature increases, as the gas becomes more oxidizing, or both. For example, because curve a was produced at lower temperatures and more reducing conditions than curve c, it is anticipated that, had the experiment that produced curve a been run for a longer time, weight loss would have eventually been observed, exhibiting curve c behavior. Finally, we note that after exposure of a freshly polished wafer to conditions where its weight change follows curve c, its subsequent weight change pattern remains unchanged. Once a silica layer is formed, the weight loss of the wafer will follow curve b, even under conditions where freshly polished wafers initially gain weight (curve c).

More detailed experiments were performed under three sets of conditions to maximize our ability to determine oxidation mechanisms and to be able to extrapolate our results to various nebular and planetary environments. The first set of experiments was at IW-2.8, where, based on Figure 3, "instantaneous" weight loss of SiC occurs even on fresh SiC wafers for temperatures exceeding ~1200°C. The second set was at IW-6.0, which approximates the oxygen fugacity of a gas of solar composition, and the third set was conducted at a constant temperature of 1300°C but variable oxygen fugacity. This temperature was deemed high enough that the weight loss rate could be determined in a reasonable period of time but low enough to minimize sample degradation. Sample characteristics, experimental conditions, and measured rates of weight changes are presented in Table 2. Examination of this table shows that volatilization rates of polycrystalline β-SiC and single crystal α-SiC at the same temperature are identical to one another within experimental errors at log fO_2 of IW-2.0 and IW-6.0.

3.2.2. Kinetics of SiC Volatilization in H_2-CO_2 at log fO_2 = IW-2.8

Results of experiments on polycrystalline β-SiC at IW-2.8 are given in Table 2. Each series of experiments began with either a freshly polished wafer or one that had been used previously in our short reconnaissance experiments under oxidizing (>IW-2.8) conditions. In each case, weight loss was linear with time throughout the experiment (cf. curve b in Fig. 4). Figure 5 shows typical results for a single β-SiC wafer run at IW-2.8. The weight loss at this fO_2 is a linear function of time even after ~25 h at 1248°C and after the loss of more than 1 mg (~10% of total mass, corresponding to the removal of an ~8-μm-thick SiC layer from each surface) at 1501°C. The same behavior was observed for different wafers, with weight loss rates at the same conditions being reproducible within 13%. For example, five experiments on four different wafers of β-SiC run at IW-2.8, 1398 $\pm$ 4°C, and gas flow rate 1.0 cm/s yielded a mean weight loss rate of $(1.5 \pm 0.2) \times 10^{-5}$ mg/min/mm^2. The linearity of weight loss with time, systematic changes in the weight loss with temperature, and reproducibility of the results for different wafers indicate that it is a chemical process rather than physical breakage of tiny chips of material from wafers that is responsible for the observed weight loss.

After exposure of a fresh SiC wafer to an H_2-CO_2 gas mixture at IW-2.8 for ~1 h at ~1400°C, the surface of the wafer becomes uniformly iridescent to the eye. SEM examination shows that the surface is very smooth without visible pits or grain boundaries, but TEM examination of a specimen exposed for ~98 h at 1197 to 1501°C (Fig. 6a) reveals a ~0.75- to 1.0-μm-thick layer of cristobalite, identified from selected area diffraction patterns. The presence of a silica layer on the SiC surface was confirmed by RBS. Figure 6b shows a typical RBS spectrum obtained from a β-SiC wafer with an iridescent layer formed after ~21 h at 1400°C. Data appear as points, and the curve represents the spectral simulation of a single silica layer, 0.1 μm thick, on a SiC substrate. The simulation provides a good fit to the observed spectrum except at low energies where the theoretical basis for the simulation fails (Doolittle, 1985). The trailing edge of the oxygen peak clearly indicates that carbon exists beneath, or mixed with, the silica layer near the oxide–carbide internal interface, which is consistent with results of Cooper and Chyung (1987) for anorthite-SiC and spodumene-SiC interfaces. The thinner silica layer in Figure 6b relative to that in Figure 6a might reflect a shorter exposure time to reactive gas mixtures and a lower maximum temperature. We conclude on the basis of morphologic and chemical examination of the SiC wafers that even when SiC loses weight throughout an experiment at IW-2.8, there is a thin but continuous silica layer on the surface. Therefore, volatilization of SiC at IW-2.8 probably occurs via a mechanism involving a surface layer of silica. The initial period of weight gain required to produce the silica layer is apparently shorter than the shortest duration of wafer exposure in our experiments (10 min).

Linearity of the data plotted in Figure 5, as well as in all other experiments at IW-2.8, has two important implications. First, it suggests that changes in effective surface area of the wafers during the experiments are relatively small. This is supported by the fact that the weight loss rate of a freshly polished wafer (e.g., $(1.8 \pm 0.1) \times 10^{-5}$ mg/min/mm^2 at 1402°C) is very similar to the rate obtained at 1394°C on the same wafer ($(1.4 \pm 0.1) \times 10^{-5}$ mg/min/mm^2) after exposure to the gas mix for nearly 100 h and loss of ~2.2 mg or 17% of its weight, which corresponds to the removal of an ~18 μm thick SiC layer from each surface. This is not surprising, as even a weight loss this extreme would correspond to only a few percent decrease in surface area, if there is no surface roughening and the relative changes in all wafer dimensions are the same. Thus, the initial surface area can be used to normalize reaction rates even after extensive exposure of the wafers to reactive gases at IW-2.8. Second, the linearity suggests one of two possible rate-limiting steps: (a) an interface-controlled reaction or (b) the supply of a gaseous reactant to and/or removal of a gaseous product from the surface of SiC (e.g.,

Table 2. Sample characteristics, experimental conditions and measured volatilization rates of silicon carbide.

Sample[a]	Orientation[b]	Initial weight (mg)	Initial surface area[c] (mm^2)	Temperature (°C)	Gas mixture	log fO_2	Gas flow rate (cm/s)	Run duration (min)	Total weight loss (mg)	Volatilization rate[c] (mg/min/mm^2)	Comments[d]
CVD #2F	∥	14.928	39.0 ± 0.8	1399	H_2-CO_2	IW-2.8	0.5	901	0.483	(1.4 ± 0.1)e-5	Fresh wafer
				1399	H_2-CO_2	IW-2.8	0.9	551	0.319	(1.5 ± 0.1)e-5	
				1399	H_2-CO_2	IW-2.8	1.6	769	0.442	(1.5 ± 0.1)e-5	
				1399	H_2-CO_2	IW-2.8	0.8	506	0.263	(1.5 ± 0.1)e-5	
				1399	H_2-CO_2	IW-2.8	0.3	828	0.421	(1.3 ± 0.1)e-5	
CVD #3A3(1)	⊥	10.676	36.2 ± 2.0	1399	H_2-CO_2	IW-2.8	1.1	934	0.472	(1.4 ± 0.1)e-5	Fresh wafer
CVD #3A3(2)	⊥	11.979	35.5 ± 1.4	1400	CO-CO_2	IW-2.8	1.0	1221	0.395	(9.1 ± 0.4)e-6	Fresh wafer
CVD #3A3(1)	⊥	8.648	36.2 ± 2.0	1399	H_2-CO_2	IW-2.8	1.0	966	0.494	(1.4 ± 0.1)e-5	Used wafer
CVD #2T	∥	14.259	39.1 ± 0.6	1203	H_2-CO_2	IW-2.0	1.1	3604	0.005	(3.5 ± 0.2)e-8	Fresh wafer
				1396	H_2-CO_2	IW-2.8	1.1	81	0.048	(1.4 ± 0.1)e-5	
CVD #1Bb	⊥	13.766	39.3 ± 1.2	1402	H_2-CO_2	IW-2.8	1.0	257	0.179	(1.8 ± 0.1)e-5	Fresh wafer
				1300	H_2-CO_2	IW-2.8	1.0	991	0.050	(1.3 ± 0.1)e-5	
				1197	H_2-CO_2	IW-2.8	1.0	1201	0.002	(4.7 ± 0.9)e-8	
				1248	H_2-CO_2	IW-2.8	1.0	1499	0.019	(3.3 ± 0.2)e-7	
				1347	H_2-CO_2	IW-2.8	1.0	844	0.163	(4.9 ± 0.1)e-6	
				1501	H_2-CO_2	IW-2.8	1.0	164	1.037	(1.6 ± 0.1)e-4	
				1448	H_2-CO_2	IW-2.8	1.0	202	0.387	(4.9 ± 0.1)e-5	
				1394	H_2-CO_2	IW-2.8	1.0	696	0.368	(1.4 ± 0.1)e-5	
CVD #4-3	∥	13.213	38.3 ± 0.3	1296	H_2-CO_2	IW-6.0	0.4	74	0.004	(1.2 ± 0.4)e-6	Fresh wafer
				1296	H_2-CO_2	IW-6.0	1.2	163	0.010	(1.7 ± 0.1)e-6	
				1296	H_2-CO_2	IW-6.0	0.8	222	0.017	(2.0 ± 0.1)e-6	
CVD #2N	∥	17.161	40 ± 2.2	1198	H_2-CO_2	IW-6.0	1.0	1934	0.006	(7.7 ± 2.6)e-8	Fresh wafer
				1246	H_2-CO_2	IW-6.0	1.0	1599	0.020	(3.1 ± 0.2)e-7	
				1298	H_2-CO_2	IW-6.0	1.0	1117	0.081	(1.8 ± 0.1)e-6	
				1396	H_2-CO_2	IW-6.0	1.0	944	1.017	(2.7 ± 0.2)e-5	
				1488	H_2-CO_2	IW-6.0	1.0	148	2.086	(3.5 ± 0.1)e-4	
				1231	H_2-CO_2	IW-6.0	1.0	788	0.017	(5.2 ± 1.1)e-7	
CVD #2P	∥	18.92	40.8 ± 1.6	1389	H_2-CO_2	IW-6.0	1.0	286	0.156	(1.3 ± 0.1)e-5	Fresh wafer
				1231	H_2-CO_2	IW-6.0	1.0	814	0.007	(2.0 ± 0.2)e-7	
				1486	H_2-CO_2	IW-6.0	1.0	63	0.527	(2.0 ± 0.1)e-4	
SC #3Ce	Unknown	13.378	33.9 ± 1.0	1229	H_2-CO_2	IW-6.0	1.0	1895	0.009	(1.4 ± 0.4)e-7	Fresh wafer
				1386	H_2-CO_2	IW-6.0	1.0	266	0.101	(1.1 ± 0.1)e-5	
				1485	H_2-CO_2	IW-6.0	1.0	59	0.477	(2.4 ± 0.1)e-4	
				1279	H_2-CO_2	IW-6.0	1.0	811	0.037	(1.3 ± 0.1)e-6	
CVD #2Qa	⊥	19.371	41.5 ± 1.0	1295	CO-CO_2	IW-6.0	1.1	569	0.024	(1.0 ± 0.1)e-6	Fresh wafer
				1395	CO-CO_2	IW-6.0	1.1	418	0.317	(1.9 ± 0.2)e-5	
CVD #2Qb	⊥	15.919	40.3 ± 0.9	1395	H_2-7.6% CO-0.1% CO_2	IW-6.0	1.1	2232	1.974	(2.2 ± 0.1)e-5	Fresh wafer
CVD #2Qe	⊥	9.033	39.0 ± 1.1	1387	H_2-CO_2	IW-6.0	1.1	82	0.056	(1.7 ± 0.1)e-5	Fresh wafer
CVD #2Rb	⊥	12.379	38.4 ± 1.3	1390	H_2-CO_2	IW-6.0	1.1	63	0.028	(1.2 ± 0.1)e-5	Fresh wafer
CVD #2Qc	⊥	13.766	39.8 ± 0.9	1437	H_2-CO_2	IW-0.3	1.1	1323	0.067	(1.1 ± 0.1)e-6	Fresh wafer; first measurement ~4 h after initial exposure
				1437	H_2-CO_2	IW-6.0	1.1	738	3.170	from 3.6e-4 to 5.9e-5	Nonlinear weight loss (see text)
CVD #2Qd	⊥	14.535	40.1 ± 1.2	1437	H_2-CO_2	IW-0.3	1.1	128	0.000	(1.4 ± 0.1)e-6	Fresh wafer; gained weight over 35 min (~0.006 (mg), then weight loss
				1437	H_2-CO_2	IW-6.0	1.1	257	0.312	from 1.8e-4 to 2.5e-5	Nonlinear weight loss (see text)
CVD #4–14	∥	19.018	40.8 ± 1.5	1346	H_2-CO_2	IW-6.0	1.1	105	0.019	(4.5 ± 0.9)e-6	Fresh wafer; initial rate
								353	0.103	(7.2 ± 0.4)e-6	Final rate
CVD #4–15	∥	25.982	43.3 ± 2.2	1345	H_2-CO_2	IW-6.0	1.1	248	0.048	(4.5 ± 0.4)e-6	Fresh wafer
CVD #4–15	∥	23.631	41.1 ± 2.8	1345	H_2-CO_2	IW-6.0	1.1	143	0.020	(3.4 ± 0.3)e-6	Repolished; initial rate
								195	0.038	(4.7 ± 0.4)e-6	Final rate
CVD#4–22a	⊥	15.964	53.0 ± 0.7	1344	H_2-CO_2	IW-6.0	1.1	2830	1.120	(7.7 ± 0.2)e-6	Fresh wafer
CVD #4–12	∥	16.772	39.6 ± 1.2	1252	H_2-CO_2	IW-6.0	1.1	1403	0.017	(2.9 ± 0.2)e-7	Fresh wafer
CVD #4–22c	⊥	37.966	81.2 ± 2.3	1252	H_2-CO_2	IW-6.0	1.1	1652	0.058	(4.1 ± 0.4)e-7	Fresh wafer
CVD #4–23a(1)	⊥	14.258	47.8 ± 2.2	1346	H_2-CO_2	IW-6.0	1.1	183	0.040	(4.1 ± 0.4)e-6	Fresh wafer; initial rate
								777	0.357	(9.6 ± 0.4)e-6	Final rate
CVD #4–23a(2)	⊥	13.247	45.6 ± 1.2	1345	H_2-CO_2	IW-6.0	1.1	284	0.068	(5.3 ± 0.4)e-6	Fresh wafer; initial rate
								202	0.088	(9.5 ± 0.5)e-6	Final rate
CVD #4–23b(1)	⊥	21.649	47.6 ± 1.9	1345	H_2-CO_2	IW-6.0	1.1	61	0.013	(4.3 ± 0.7)e-6	Fresh wafer; initial rate
								158	0.049	(6.6 ± 0.3)e-6	Final rate

(Continued)

Table 2. (Continued)

Sample[a]	Orientation[b]	Initial weight (mg)	Initial surface area[c] (mm^2)	Temperature (°C)	Gas mixture	log fO_2	Gas flow rate (cm/s)	Run duration (min)	Total weight loss (mg)	Volatilization rate[c] (mg/min/mm^2)	Comments[d]
CVD #4–23a(3)	⊥	11.222	42.1 ± 1.4	1345	H_2-CO_2	IW-6.0	1.1	83	0.019	(5.4 ± 0.2)e-6	Fresh wafer; initial rate
								982	0.355	(8.6 ± 0.2)e-6	Final rate
CVD #4–23b(2)	⊥	16.716	48.4 ± 1.2	1344	H_2-CO_2	IW-6.0	1.1	126	0.035	(5.7 ± 0.4)e-6	Fresh wafer; initial rate
								817	0.341	(8.7 ± 0.2)e-6	Final rate
CVD #4-23b(3)	⊥	15.406	48.4 ± 1.5	1344	H_2-CO_2	IW-6.0	1.1	146	0.024	(3.3 ± 0.2)e-6	Fresh wafer; initial rate
								217	0.054	(5.2 ± 0.4)e-6	Final rate
CVD #4-24a	⊥	24.335	44.9 ± 0.5	1345	H_2-CO_2	IW-6.0	1.1	271	0.044	(3.7 ± 0.2)e-6	Fresh wafer; initial rate
								129	0.036	(6.3 ± 0.1)e-6	Final rate
CVD #4-24b	⊥	19.888	40.2 ± 1.2	1250	H_2-CO_2	IW-6.0	1.1	952	0.012	(3.2 ± 0.2)e-7	Fresh wafer
				1300	H_2-CO_2	IW-6.0	1.1	466	0.035	(1.8 ± 0.2)e-6	
				1201	H_2-CO_2	IW-6.0	1.1	598	0.003	1.2e-7	Rate based on two weight measurements
				1400	H_2-CO_2	IW-6.0	1.1	90	0.131	(3.6 ± 0.2)e-5	
SC #3Gf	Unknown	20.429	49.7 ± 1.3	1350	H_2-CO_2	IW-6.0	1.1	481	0.146	(6.1 ± 0.2)e-6	Fresh wafer
SC #3–3	Unknown	8.996	35.9 ± 0.8	1300	H_2-CO_2	IW-2.0	1.2	2306	0.045	(5.7 ± 0.2)e-7	Fresh wafer
				1250	H_2-CO_2	IW-2.0	1.2	2905	0.019	(1.9 ± 0.1)e-7	
				1348	H_2-CO_2	IW-2.0	1.2	390	0.025	(1.8 ± 0.1)e-6	
				1277	H_2-CO_2	IW-2.0	1.2	2080	0.024	(3.4 ± 0.3)e-7	
				1322	H_2-CO_2	IW-2.0	1.2	746	0.026	(9.8 ± 0.5)e-7	
				1299	H_2-CO_2	IW-2.0	1.2	2155	0.044	(5.7 ± 0.4)e-7	
CVD #5-1	∥	7.055	37.2 ± 1.4	1299	H_2-CO_2	IW-2.0	1.2	1191	0.022	(5.7 ± 0.4)e-7	Fresh wafer; first 80 min weight gain (~0.002 mg), then weight loss
				1249	H_2-CO_2	IW-2.0	1.2	2845	0.020	(1.9 ± 0.2)e-7	
				1348	H_2-CO_2	IW-2.0	1.2	350	0.027	(2.1 ± 0.2)e-6	
				1322	H_2-CO_2	IW-2.0	1.2	1183	0.038	(8.9 ± 0.6)e-6	
SC #3–5	Unknown	23.277	42.4 ± 0.6	1300	H_2-CO_2	IW+1.0	1.1	3860	0.101	(7.3 ± 0.5)e-7	Fresh wafer; first 180 min weight gain (~0.004 mg), then weight loss
SC #3-1	Unknown	10.530	33.0 ± 0.4	1301	H_2-CO_2	IW-4.3	1.1	799	0.025	(9.7 ± 3.6)e-7[e]	Fresh wafer; initial rate
								1194	0.117	(3.3 ± 0.7)e-6	Final rate
				1301	H_2-CO_2	IW-5.5	1.1	349	0.031	(8.7 ± 1.7)e-7[f]	
				1301	H_2-CO_2	IW-4.9	1.1	419	0.038	(9.1 ± 1.9)e-7[f]	
				1301	H_2-CO_2	IW-6.0	1.1	300	0.039	(1.3 ± 0.3)e-6[f]	
				1301	H_2-CO_2	IW-5.2	1.1	274	0.034	(1.2 ± 0.3)e-6[f]	
				1301	H_2-CO_2	IW-5.7	1.1	463	0.070	(1.5 ± 0.3)e-6[f]	
				1301	H_2-CO_2	IW-5.5	1.1	65	0.010	(1.5 ± 0.3)e-6[f]	
				1301	H_2-CO_2	IW-5.2	1.1	60	0.009	(1.5 ± 0.3)e-6[f]	
				1301	H_2-CO_2	IW-4.9	1.1	71	0.009	(1.4 ± 0.3)e-6[f]	Initial rate
								32	0.009	2.7e-6[f]	Final rate; rate based on two weight measurements
				1301	H_2-CO_2	IW-5.5	1.1	200	0.047	(1.2 ± 0.3)e-6[g]	
				1301	H_2-CO_2	IW-7.4	1.1	93	0.094	(4.8 ± 1.3)e-6[g]	
				1301	H_2-CO_2	IW-5.9	1.1	119	0.036	(1.5 ± 0.4)e-6[g]	
				1301	H_2-CO_2	IW-6.2	1.1	88	0.025	(1.4 ± 0.3)e-6[g]	
				1301	H_2-CO_2	IW-8.9	1.1	55	0.066	(6.0 ± 1.5)e-6[g]	
				1301	H_2-CO_2	IW-6.7	1.1	107	0.043	(2.0 ± 0.5)e-6[g]	
				1301	H_2-CO_2	IW-10.4	1.1	55	0.162	(1.5 ± 0.3)e-5[g]	
				1301	H_2-CO_2	IW-5.9	1.1	520	0.184	(1.7 ± 0.3)e-6[g]	
SC #4-2-1	Unknown	19.645	45.3 ± 1.1	1297	H_2-CO_2	IW-5.1	1.0	415	0.021	(1.2 ± 0.1)e-6	Fresh wafer
				1300	H_2-CO_2	IW-5.9	1.0	280	0.025	(2.0 ± 0.1)e-6	
SC #4-3-1	Unknown	33.478	41.0 ± 0.4	1300	H_2-CO_2	IW-4.5	1.0	410	0.024	(1.4 ± 0.1)e-6	Fresh wafer
				1300	H_2-CO_2	IW-6.6	1.0	187	0.015	(2.2 ± 0.1)e-6	
				1300	H_2-CO_2	IW-7.5	1.0	115	0.021	(4.4 ± 0.2)e-6	

(Continued)

Table 2. (Continued)

Sample[a]	Orientation[b]	Initial weight (mg)	Initial surface area[c] (mm^2)	Temperature (°C)	Gas mixture	log fO_2	Gas flow rate (cm/s)	Run duration (min)	Total weight loss (mg)	Volatilization rate[c] (mg/min/mm^2)	Comments[d]
				1300	H_2-CO_2	IW-3.5	1.0	305	0.025	(2.0 ± 0.1)e-6	
SC #4-3-1	Unknown	28.218	38.7 ± 0.3	1300	H_2-CO_2	IW-3.9	1.0	188	0.016	(2.0 ± 0.2)e-6	Repolished wafer
				1300	H_2-CO_2	IW-7.8	1.0	185	0.030	(4.3 ± 0.3)e-6	
				1300	H_2-CO_2	IW-3.3	1.0	345	0.022	(1.7 ± 0.1)e-6	
SC #4-3-2	Unknown	24.639	31.5 ± 0.6	1301	H_2-CO_2	IW-8.5	1.0	95	0.008	(2.7 ± 0.5)e-6	Fresh wafer

[a] Sequences of experiments for each sample are given in chronological order. CVD, polycrystalline β-SiC; SC, single crystal α-SiC.
[b] Orientation of large wafer surfaces. CVD β-SiC wafers were cut perpendicular ($\perp$) or parallel ($\parallel$) to crystal growth.
[c] Uncertainties are 2σ.
[d] The notation "used wafer" indicates that the sample was used in reconnaissance experiments at or above IW-2.8 before the listed run. "Fresh wafer" refers to a pristine, freshly polished sample. "Repolished wafer" refers to a wafer that was used in a previous experiment but then repolished to remove near-surface cracks, incised grain boundaries, and silica.
[e] The volatilization rates for IW-4.3 were obtained by normalization to the initial surface area (33.0 mm^2). The difference between the initial (9.7e-7 mg/min/mm^2) and final (3.3e-6 mg/min/mm^2) rates in this run suggests that the surface area increased by a factor of three during the experiment (from 33 to 100 mm^2).
[f] A surface area of 100 ± 10 mm^2 was used to obtain the volatilization rate.
[g] A surface area of 200 ± 20 mm^2 was used to obtain the volatilization rate.

Rosner and Allendorf, 1970; Antill and Warburton, 1971; Kim, 1987; Jacobson et al., 1990).

The reason why the volatilization rate is expected to be invariant with time, even when gas transport is rate limiting, is that a boundary layer forms quickly in the gas above the wafer surface and its thickness is thereafter independent of time. Because increasing the gas flow rate usually decreases the thickness of the boundary layer and thus increases the supply rate of oxidant to and removal rate of gaseous products from the sample surface, the volatilization rate should increase continuously with gas flow rate when diffusion through the boundary layer is rate limiting. In this case, the weight loss rate should vary as the square root of gas flow rate (Bird et al., 1960; Geankoplis, 1972). On the other hand, independence of the reaction rate from gas flow rate would suggest that gaseous mass transport is faster than chemical reaction, and hence that a surface chemical reaction is rate limiting. To help distinguish between whether an interface-controlled reaction or gas phase diffusion is the rate-limiting step for SiC volatilization at IW-2.8, the SiC volatilization rate was measured as a function of gas flow rate in H_2-CO_2 mixtures. Figure 7 shows, for experiments on a single SiC wafer at 1399°C, that the SiC volatilization rate is essentially independent of flow rate, at least between ~0.5 and ~1.6 cm/s. The fact that the weight loss rate at 0.3 cm/s is slightly (~10%) lower than at 0.5 to 1.6 cm/s suggests that gas phase diffusion may become rate limiting at very low flow rates. Unfortunately, we were unable to measure and control gas flow rates accurately below 0.3 cm/s due to convection in the furnace tube, so we cannot completely rule out this possibility. Low flow rates can also lead to serious wall effects, which would complicate interpretation of experimental results. Our results agree in part with those of Kim (1987) and Kim and Readey (1989), who showed that within the range of flow rates studied (~0.3 to 2 cm/s), the SiC volatilization rates in H_2-H_2O gas mixtures with $P_{H_2O} < 10^{-3}$ atm is independent of gas flow rates at temperatures below 1327°C, and increases by about a factor of two at 1527°C. Most of our experiments were conducted at gas flow rates of 1.0 and 1.1 cm/s where the rate-limiting step is the interface reaction. The issue of whether gas phase diffusion can be rate limiting under solar nebular conditions is addressed in Section 4.4.

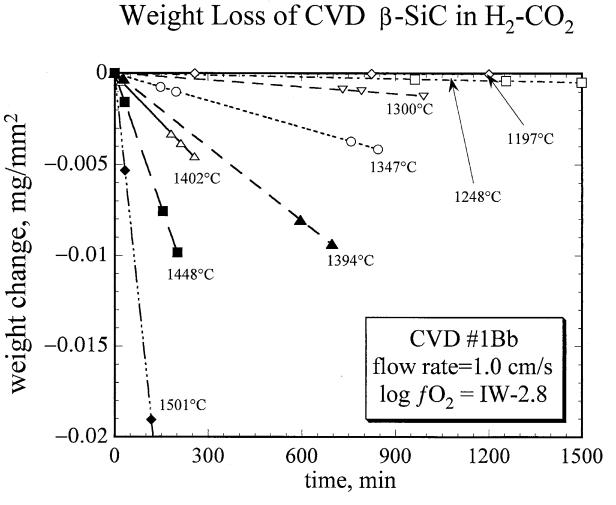

Fig. 5. Weight change of polycrystalline β-SiC (CVD #1Bb) normalized to initial surface area (39.3 mm^2) that was exposed to H_2-CO_2 gas mixtures at IW-2.8 with an inlet gas flow rate of 1.0 cm/s. The first and last runs were conducted at 1402 and 1394°C, respectively. All of the experiments are consistent with a linear weight loss as a function of time.

An additional clue to the mechanism is provided by the activation energy for SiC volatilization, obtained from the temperature dependence of the weight loss rate. In Figure 8, the logarithm of the weight loss rate for experiments conducted at a gas flow rate of 1.0 to 1.2 cm/s (Table 2) is plotted against the reciprocal of temperature. The linear relationship exhibited by the data at IW-2.8 is consistent with a single mechanism for volatilization of SiC over the entire temperature range encompassed by the experiments (1197 to 1501°C). The apparent activation energy of CVD β-SiC volatilization calculated from the slope of the line at IW-2.8 is $E_a = 563 \pm 8$ (1σ) kJ/mol of

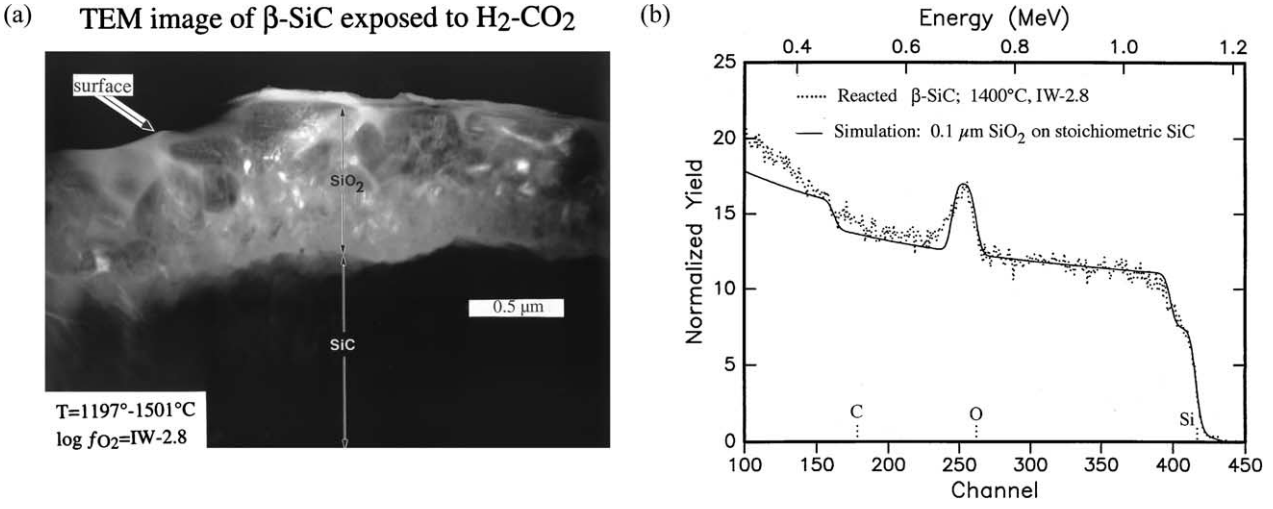

Fig. 6. (a) TEM image of the near-surface region of a β-SiC wafer (CVD #1Bb) exposed to H_2-CO_2 at IW-2.8 for 108 h in the temperature range 1197 to 1501°C. (b) RBS spectrum of a β-SiC wafer exposed to 50% (He, Ne, Ar)-H_2-CO_2 at IW-2.8 for 21 h at 1400°C. Energy positions for elastic collisions at the free surface of the specimen are indicated at the top of the figure. Expected positions for C, O, and Si are indicated along the x-axis. The curve represents a spectral simulation for a 0.1-μm-thick layer of SiO_2 on an SiC surface.

SiC consumed. This is indistinguishable from the value of 548 kJ/mol obtained by Pultz and Hertl (1966) at temperatures below 1380°C for the reaction

$$2SiO_{2(s)} + SiC_{(s)} \rightarrow 3SiO_{(g)} + CO_{(g)} \quad (7)$$

but higher than 405 kJ/mol obtained at temperatures higher than 1380°C. Our experimentally determined value of E_a obtained from experiments conducted at 1400°C and below is therefore consistent with reaction 7 being responsible for weight loss of SiC at IW-2.8, at least at temperatures below ~1400°C.

3.2.3. *Kinetics of SiC Volatilization at log fO_2 = IW-6.0*

SEM examination shows that wafers of both polycrystalline CVD β-SiC and single crystal α-SiC from experiments at IW-6.0 have highly irregular surfaces, in contrast to the smooth, iridescent surfaces produced at IW-2.8. Pits and incised grain boundaries are common, and qualitatively, the surface roughness increases with run duration and temperature for experiments above 1300°C. The CVD β-SiC wafers appear to be more irregular than single crystal α-SiC run under similar conditions. TEM images (Fig. 9a) revealed no silica layers

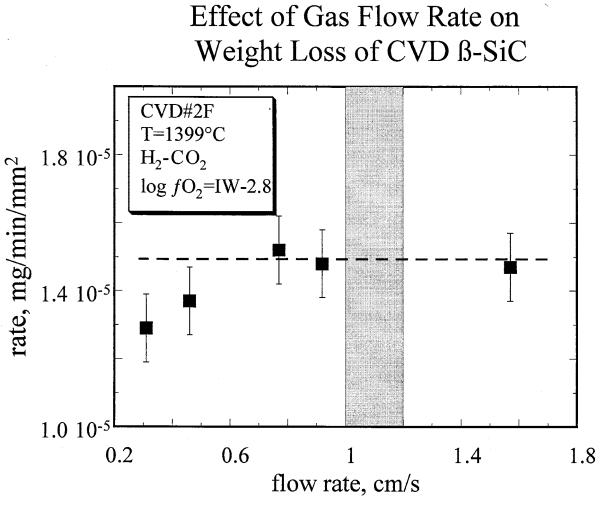

Fig. 7. Dependence of SiC weight loss rate on flow rate in H_2-CO_2 gas mixtures at IW-2.8 at 1400°C (CVD #2F). A line showing the average reaction rate for experiments conducted at flow rates exceeding 0.7 cm/s is also shown. Shaded region (1.0 to 1.2 cm/s) encompasses typical flow rates for SiC experiments in this study.

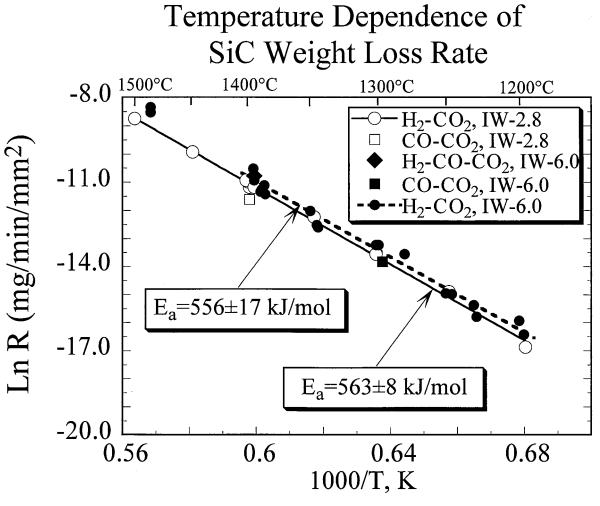

Fig. 8. Temperature dependence of SiC weight loss rate, R, in H_2-CO_2, CO-CO_2 and in H_2-CO-CO_2 gas mixtures at IW-2.8 and IW-6.0. A regression line for IW-2.8 is shown as a solid line. The dashed line is a regression for all IW-6.0 data on wafers that were never exposed to temperatures above 1400°C at IW-6, excluding those for CVD #2Qc, CVD #2Qd, and SC #3-1 (see text).

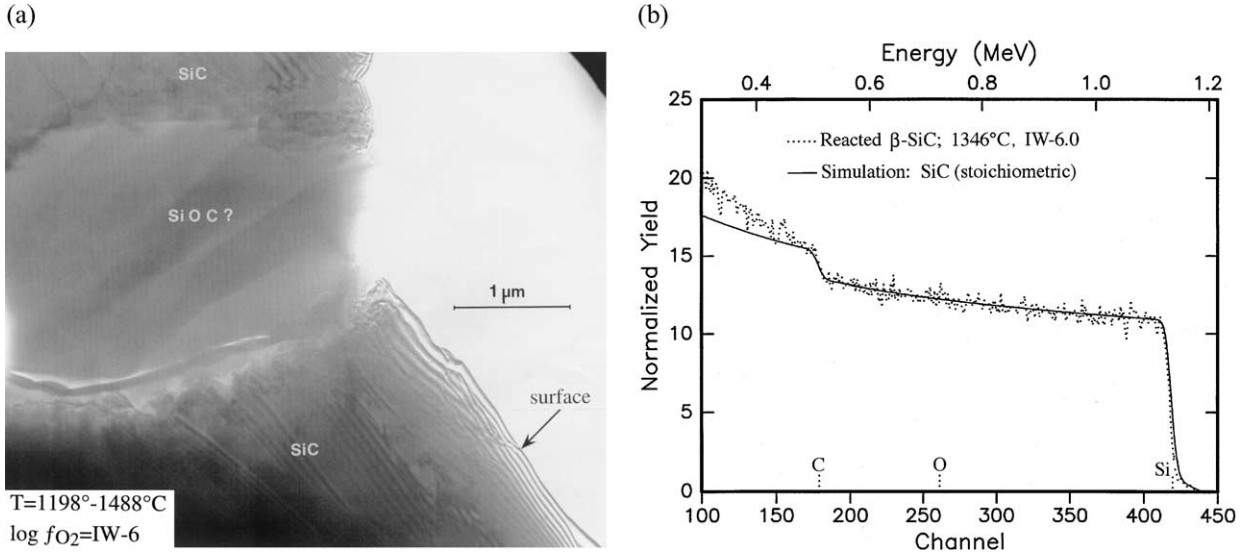

Fig. 9. (a) TEM image of the near-surface region of a β-SiC wafer (CVD #2N) exposed to H_2-CO_2 with log fO_2 = IW-6.0 for 109 h at 1198 to 1488°C. The surface lacks a visible silica layer, but Si-, O-, and C-bearing material is observed as filling in pits. (b) RBS spectrum of SiC wafer (CVD #4-23a) exposed to the same gas mixture for 16 h at 1346°C.

analogous to those observed for experiments at IW-2.8 (Fig. 6a), although analytical TEM yields evidence for Si- and O-bearing material inside pits. Similarly, RBS spectra of the wafers can be modeled as arising from pure SiC (Fig. 9b), which limits any surface layer of silica to a thickness of less than 0.01 μm.

Although surface morphologies for SiC samples reacted at IW-2.8 and IW-6.0 in H_2-CO_2 gas mixtures are quite different, the reaction kinetics are similar. Weight losses in most experiments at IW-6.0 (up to ~3.2 mg for CVD #2N, corresponding to the removal of an ~25-μm-thick layer of SiC from each surface) are a linear function of time (Fig. 10), and weight loss rates are reproducible in short duration experiments up to 1400°C. In some extended experiments with polycrystalline CVD β-SiC at temperatures above 1300°C (Fig. 11, Table 2), however, the slopes of the weight loss curves increased by more than a factor of two, leading to a corresponding increase in SiC volatilization rate when the initial geometric surface area is used for normalization. These changes in slope were usually very abrupt, as shown in Figure 11. Both optical and SEM examination of such wafers reveal highly irregular surfaces compared to wafers that were never exposed to IW-6.0 at high temperatures for an extended period of time. Kim (1987), Jacobson et al. (1990), and Kim and Moorhead (1990) also observed severe degradation of surfaces of different types of SiC under reducing conditions and showed that it is higher for polycrystalline than for single crystal SiC. If the change in weight loss rate were due to a change in the reaction mechanism, then all long-duration experiments should have reproducible weight loss rates. In long runs, however, weight loss rates varied significantly, and these variations were higher for polycrystalline samples than for single crystals. This suggests that increases in calculated weight loss rates normalized to the initial surface area more likely reflect increases in the wafer surface area due to sample degradation than changes in the reaction mechanism with time. Therefore, although both initial and final rates normalized to initial surface area are given in Table 2, when a change in the weight loss rate at given temperature was observed in an SiC experiment at IW-6.0, only the initial weight loss rate was used. We were unable to measure precisely initial weight loss rates at ~1490°C due to extremely high rates and severe damage to the wafer surfaces. This suggests an increase by a factor of two or more in the wafer surface area over the course of a few hours' exposure.

In Figure 8, the dashed line for IW-6.0 is obtained for relatively short duration experiments on both CVD β-SiC and single crystal α-SiC, the results for which are indistinguishable. Data at ~1490°C are ignored due to sample degradation. The weight loss rates for SiC at IW-6.0 are generally slightly higher than but within 2σ of those observed at IW-2.8 (e.g., at 1400°C,

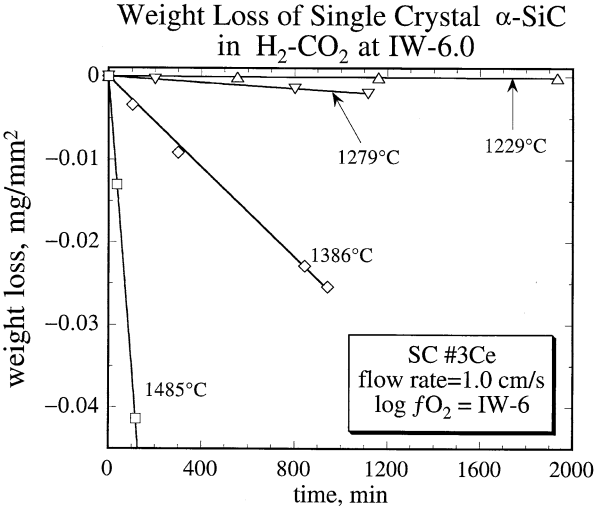

Fig. 10. Weight loss of α-SiC (SC #3Ce) in H_2-CO_2 at IW-6.0 and a flow rate of 1.0 cm/s at various temperatures.

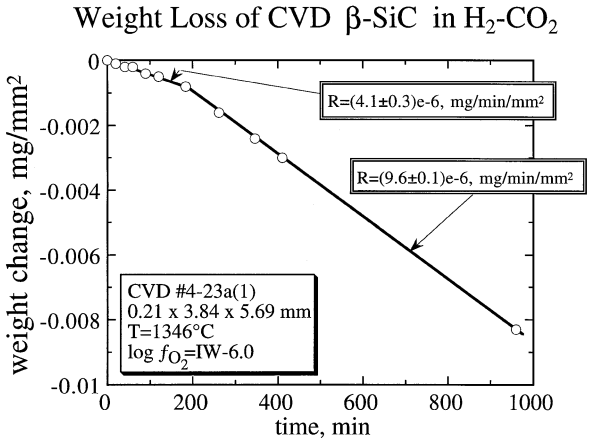

Fig. 11. Weight loss of CVD β-SiC in H_2-CO_2. An example of an abrupt change in the weight loss rate during volatilization of CVD β-SiC. After 3 h of exposure to H_2-CO_2 at IW-6.0, the weight loss rate suddenly increased by ~2.5 times.

the average rate ($\pm 2\sigma$) interpolated from the best fit of the whole data set in H_2-CO_2 is $(2.0 \pm 0.9) \times 10^{-5}$ mg/min/mm^2 at IW-6.0 and $(1.5 \pm 0.2) \times 10^{-5}$ at IW-2.8), despite the fact that partial pressures of all major oxygen-bearing species (H_2O, CO, CO_2) differ by more than a factor of ~40 (Fig. 2a).

SiC wafers exposed to 92.3% H_2 + 7.6% CO + 0.1% CO_2 and to CO-CO_2 gas mixtures at IW-6.0 also lost weight as a linear function of time, and the rates of weight loss (e.g., $(2.2 \pm 0.1) \times 10^{-5}$ in H_2-CO-CO_2 and $(1.9 \pm 0.1) \times 10^{-5}$ mg/min/mm^2 in CO-CO_2 at 1395°C) are similar to those for H_2-CO_2 at the same temperature (Table 2, Fig. 8). This suggests that the same volatilization mechanism operates in all gas mixtures used at IW-6.0. Because the volatilization rates for IW-2.8 and IW-6.0 are similar at each temperature, the temperature dependences are also very similar. The best-fit activation energy based on the data plotted in Figure 8 are 556 ± 17 kJ/mol at IW-6.0 (excluding wafers exposed to 1490°C), which is indistinguishable from 563 ± 8 kJ/mol at IW-2.8. The same activation energies at IW-6.0 and IW-2.8 suggest that the mechanism of SiC volatilization may be also the same, despite the existence of a thin surface layer of silica at IW-2.8 and the apparent lack of one at IW-6.0.

3.2.4. Dependence of SiC Volatilization Kinetics on fO_2 at 1300°C

The volatilization rates of several wafers of single crystal α-SiC (SC #3-1, SC #3-3, SC #4-2-1, SC #4-3-1, and SC #4-3-2) were measured in H_2-CO_2 gas mixtures at ~1300°C and oxygen fugacities ranging from 7.4×10^{-22} to 1.9×10^{-13}, corresponding to IW-10.4 to IW-2.0 (Table 2). Weight loss for all experiments was a linear function of time at each fO_2 over the entire range of oxygen fugacities studied except for two runs for wafer SC #3-1. In the first run at IW-4.3, the weight loss rate of the freshly polished wafer increased continuously for 32 h. The increase in the weight loss rate was accompanied by an increase in surface roughness. The difference between the initial and final volatilization rates at IW-4.3 (9.7×10^{-7} and 3.3×10^{-6} mg/min/mm^2), obtained by normalizing the weight loss for SC #3-1 to the initial surface area of 33.0 mm^2, suggests that an increase in wafer surface area by about a factor of three could be responsible for the change. Therefore, rates for the next eight experiments (up to the one at IW-4.9, Table 2) were obtained by normalizing to a surface area of 100 mm^2. The linearity of the weight loss with time within each of these eight, relatively short runs suggests that any changes in wafer surface area were too low to affect the volatilization rate. After ~67 h of total exposure time during the second experiment at IW-4.9, the weight loss rate increased sharply by a factor of two: the initial weight loss rate, $(1.4 \pm 0.3) \times 10^{-6}$ mg/min/mm^2, which was the same within error of the rate for the first experiment at IW-4.9, $(0.9 \pm 0.2) \times 10^{-6}$, increased to 2.7×10^{-6} mg/min/mm^2. We suggest that this change in weight loss rate may be caused by an increase in surface area (opening up internal pore space?) by the same amount, although we cannot confirm this. The weight loss in all succeeding experiments was normalized to 200 mm^2.

The results are shown in Figure 12. Also shown are data for SiO_2 at 1300°C, which are discussed in the following section, and averaged rates for SiC at IW-2.8 and IW-6.0 obtained from the regression lines plotted in Figure 8. For log fO_2 between ~IW-3 and ~IW-6, volatilization rates of single crystal α-SiC cluster along a line of constant rate (1.5×10^{-6} mg/min/mm^2) with no sign of systematic variations. This result confirms those discussed above on the basis of a comparison of weight loss rates at IW-2.8 and IW-6.0, obtained by means of different SiC wafers in each experiment (Fig. 8). Outside this range of oxygen fugacities, however, the SiC volatilization rate becomes strongly fO_2 dependent both to more oxidizing and to more reducing conditions. Under more oxidizing conditions (~IW-3 to ~IW-2), the weight loss rate decreases with increasing fO_2 and compares favorably to the volatilization rate of silica glass (discussed in the next section). Under more reducing conditions, the SiC volatilization rate increases with decreasing fO_2 by an order of magnitude between ~IW-6 and IW-10.4. Exactly the same relationship as shown in Figure 12 is observed if volatilization rate is plotted as a function of the partial pressure of any other oxidizing species (CO_2, H_2O, OH, etc.). These results are qualitatively consistent with those of Kim and Readey (1989) and Kim and Moorhead (1990) on the volatilization of hot-pressed α-SiC in H_2-H_2O mixtures. In their experiment at 1400°C, for example, the volatilization rate was essentially independent of P_{H_2O}/P_{H_2} within the range from 5×10^{-3} to $\sim 2 \times 10^{-4}$, corresponding to log fO_2s from IW-4.6 to IW-7.4, then increased, reaching a maximum at $P_{H_2O}/P_{H_2} \sim 8 \times 10^{-5}$ (~IW-8.5).

3.3. Kinetics of SiO_2 Volatilization

The presence of a continuous cristobalite layer on the surface of SiC exposed to H_2-CO_2 gas mixtures at IW-2.8 suggests that SiC volatilization under these conditions might be a two-stage process involving first the formation and then the volatilization of silica. Therefore, a set of experiments was run on wafers of fused silica glass with the same apparatus and procedures described above. Samples were exposed to H_2-CO_2 gas mixtures from IW-1.0 to IW-6.0 at 1153 to 1389°C. Results are given in Table 3. Within the error of our measurements, wafers

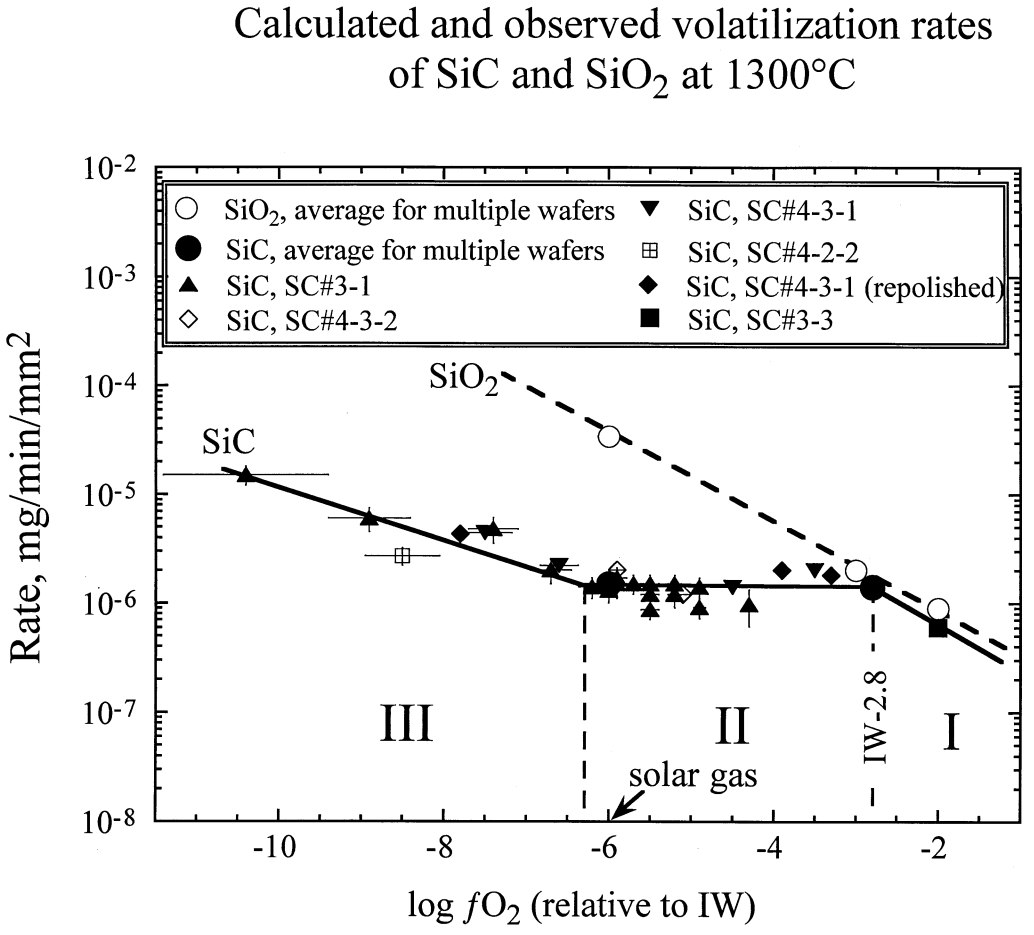

Fig. 12. Weight loss rates for a wafer of single crystal α-SiC in H_2-CO_2 as a function of fO_2 at 1300°C plotted as closed triangles. Also shown are average rates at 1300°C for multiple SiO_2 (open circles) and SiC (closed circles) wafers. The curves through the experimental data are intended only as visual aids. Roman numerals indicate redox conditions for different regimes of SiC volatilization. Uncertainties in the fO_2 measurements increase as gas becomes more reducing (Mendybaev et al., 1998).

of silica glass exposed to H_2-CO_2 lose weight throughout each experiment over the entire range of temperatures and oxygen fugacities studied. Weight loss was linear with time in all experiments (e.g., Fig. 13), except that the reaction rate for freshly polished wafers doubled after an initial exposure of ~330 min at IW-6.0 (compare the dashed, 9.5×10^{-7} mg/min/mm^2, and solid, 2.2×10^{-6} mg/min/mm^2, linear segments of the weight loss curve at 1203°C in Figure 13. A change in slope in the weight loss curve was also observed after 90 min at 1252° and ~30 min at 1387°C at IW-6.0 for newly exposed SiO_2 wafers (Table 3). No further deviations from linear weight loss with time were observed after these breaks in slope occurred, even for total exposure times exceeding 130 h. Changes in the slope of the weight loss curves most likely reflect an increase in the effective surface area of the wafers due to surface crystallization of spherulitic cristobalite (Fig. 14), although we cannot reject the possibility that silica glass and cristobalite volatilize at different rates. Cristobalite was seen previously on the surface of silica glass exposed to reducing gases by Gardner (1974) and Tso and Pask (1982). For IW-3.0 or more oxidizing conditions, optical investigation of the wafers showed no sign of surface crystallization.

The weight loss rates for SiO_2 at IW-6.0 and IW-3.0 are shown as functions of inverse temperature in Figure 15; the average rates for SiC from Figure 8 are also shown for comparison. There are two important features. First, weight loss rates for SiC and silica glass are similar for wafers exposed to ~IW-3. Second, the rate for silica at IW-6.0 is ~10 to 50 times higher than for SiO_2 at IW-3, which far exceeds the factor of two increase in SiO_2 volatilization rate ascribed above to cristobalite formation. On the other hand, no weight change was observed for an SiO_2 wafer exposed to a CO-CO_2 gas mixture at 1250°C and IW-1, even after 21 h, and only small weight losses (2 to 3 μg) occurred at 1151°C at IW-3.0 and IW-5.5 after 35 and 41 h, respectively. This indicates that the volatilization rate of SiO_2 is sensitive to gas composition and suggests that the reaction in H_2-CO_2 gas mixtures involves hydrogen-bearing species. The observed dependence of the SiO_2 volatilization rate on fO_2 in H_2-CO_2 is expected if volatilization occurs via a reaction at the SiO_2/gas interface, such as

Table 3. Sample characteristics, experimental conditions, and measured volatilization rates of silica glass.

Sample[a]	Initial weight (mg)	Initial surface area[b] (mm^2)	Temperature (°C)	Gas mixture	log fO_2	Gas flow rate (cm/s)	Run duration (min)	Total weight loss (mg)	Volatilization rate[b] ($mg/min/mm^2$)	Comments[c]
SiO_2 #1–1	8.668	38.8 ± 1.8	1387	H_2-CO_2	IW-6.0	1.1	26	0.200	(2.0 ± 0.2)e-4	Fresh wafer; initial rate
				H_2-CO_2	IW-6.0	1.1	137	1.479	(2.8 ± 0.1)e-4	Final rate
SiO_2 #1–2	24.649	47.3 ± 2.1	1389	H_2-CO_2	IW-6.0	1.3	66	0.057	1.8e-5	Fresh wafer; rate based on two weight measurements
SiO_2 #QG-1	19.621	41.1 ± 0.7	1203	H_2-CO_2	IW-6.0	1.1	332	0.013	9.5e-7	Fresh wafer; initial rate; rate based on two weight measurements
							1754	0.149	(2.2 ± 0.1)e-6	Final rate
			1299	H_2-CO_2	IW-6.0	1.1	232	0.343	(3.6 ± 0.2)e-5	
			1201	H_2-CO_2	IW-6.0	1.1	1113	0.096	(2.1 ± 0.1)e-6	
			1250	H_2-CO_2	IW-6.0	1.1	190	0.072	(9.2 ± 0.2)e-6	
			1153	H_2-CO_2	IW-6.0	1.1	974	0.019	(4.8 ± 0.4)e-7	
			1350	H_2-CO_2	IW-6.0	1.1	135	0.630	(1.1 ± 0.1)e-4	
			1201	H_2-CO_2	IW-3.0	1.1	1917	0.014	(1.8 ± 0.4)e-7	
			1350	H_2-CO_2	IW-3.0	1.1	158	0.064	(9.9 ± 0.1)e-6	
			1298	H_2-CO_2	IW-3.0	1.1	265	0.027	(2.4 ± 0.2)e-6	
			1252	H_2-CO_2	IW-3.0	1.1	837	0.025	(7.2 ± 0.2)e-7	
SiO_2 #QG-2	13.328	38.1 ± 0.8	1252	H_2-CO_2	IW-6.0	1.1	90	0.017	4.9e-6	Fresh wafer; initial rate; rate based on two weight measurements
							231	0.074	(8.3 ± 0.4)e-6	Final rate
SiO_2 #2-1	13.956	43.9 ± 1.7	1299	H_2-CO_2	IW-2.0	1.2	1409	0.056	(8.9 ± 0.4)e-7	Fresh wafer
			1249	H_2-CO_2	IW-2.0	1.2	1978	0.028	(3.2 ± 0.1)e-7	
			1348	H_2-CO_2	IW-2.0	1.2	373	0.047	(2.9 ± 0.1)e-6	
			1277	H_2-CO_2	IW-2.0	1.2	1205	0.029	(5.5 ± 0.2)e-7	
			1321	H_2-CO_2	IW-2.0	1.2	1035	0.070	(1.5 ± 0.1)e-6	
			1299	H_2-CO_2	IW-2.0	1.2	1335	0.052	(8.9 ± 0.5)e-7	
			1203	H_2-CO_2	IW-2.0	1.2	1486	0.008	(1.3 ± 0.1)e-7	
SiO_2 #2–2	31.058	53.9 ± 3.8	1300	H_2-CO_2	IW-3.0	1.2	1083	0.180	(3.2 ± 0.2)e-6	Fresh wafer
			1249	H_2-CO_2	IW-3.0	1.2	1285	0.051	(7.3 ± 0.5)e-7	
			1349	H_2-CO_2	IW-3.0	1.2	260	0.157	(1.1 ± 0.1)e-5	
SiO_2 #2–3	11.924	39.2 ± 0.6	1258	CO-CO_2	IW-1.0	1.1	1250	0.000	—	Fresh wafer; no weight change
SiO_2 #2–5	26.336	49.9 ± 2.2	1250	H_2-CO_2	IW-1.5	1.2	1457	0.031	(4.2 ± 0.3)e-7	Used wafer
SiO_2 #2–6	21.817	53.0 ± 2.3	1250	H_2-CO_2	IW-2.5	1.2	2452	0.054	(4.1 ± 0.4)e-7	Fresh wafer
SiO_2 #2–9	12.822	30.9 ± 0.3	1151	CO-CO_2	IW-3.0	1.0	2147	0.002	(2.2 ± 1.3)e-8	Fresh wafer
			1151	CO-CO_2	IW-5.5	1.0	2485	0.003	(3.5 ± 1.0)e-8	

[a] Sequences of experiments for each sample are given in chronological order.
[b] Uncertainties are 2σ.
[c] The notation "used wafer" indicates that the sample was used in reconnaissance experiments at or above IW-2.8 before the listed run. "Fresh wafer" refers to a pristine, freshly polished sample.

$$SiO_{2(s)} + H_{2(g)} \rightarrow SiO_{(g)} + H_2O_{(g)}. \quad (8)$$

Apparent activation energies for silica volatilization obtained from the slopes of the lines shown in Figure 15, are 548 ± 7 kJ/mol at IW-6.0 and 541 ± 13 kJ/mol at log fO_2 = IW-3.0, which are indistinguishable from the values for SiC, 556 ± 17 kJ/mol at IW-6.0, and 563 ± 8 kJ/mol at IW-2.8.

As a test of the role of silica in SiC volatilization at IW-6.0, we conducted experiments in which a freshly polished CVD β-SiC wafer was first exposed to H_2-CO_2 with log fO_2 = IW-0.3 at 1437°C for 2 h (CVD #2Qd) and 20 h (CVD #2Qc), to produce a layer of silica. The presence of a silica layer on each SiC wafer was indicated by a weight increase and an iridescent film over the entire surface. After these pretreatments, the wafers were removed from the furnace and the composition of the gas mixture changed to IW-6.0 while the temperature was held constant. Upon reinsertion into the furnace hot spot, the wafers immediately started to lose weight at a rate consistent with that of pure SiO_2 ($\sim 3 \times 10^{-4}$ $mg/min/mm^2$; Figs. 15 and 16). The volatilization rates gradually decreased with time, however, and after ~2 h (CVD #2Qd) and 13 h (CVD #2Qc) of exposure, the rates approached those for volatilization of a pristine wafer of SiC under the same conditions ($\sim 2 \times 10^{-5}$ $mg/min/mm^2$). The gradual decrease in volatilization rate suggests that the effective surface area of silica on SiC decreased continually during the experiment, ultimately causing a change in mechanism from one consistent with volatilization of pure silica at IW-6 to one consistent with volatilization of SiC.

4. DISCUSSION

On the basis of Figure 12, there are three distinct regimes for SiC volatilization in hydrogen-rich gas mixtures at a total

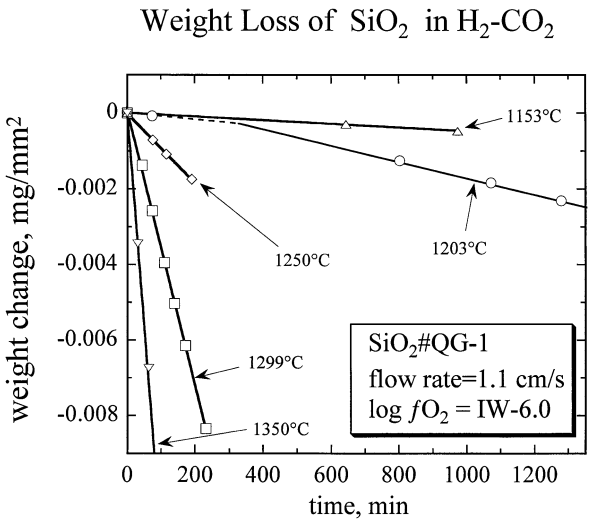

Fig. 13. Weight loss of SiO_2 (SiO_2 #QG-1) in H_2-CO_2 at IW-6.0. The first exposure of a fresh silica glass wafer to H_2-CO_2 was at 1200°C, and the change in the slope of the line for this temperature probably reflects devitrification of the surface of the sample.

pressure, P^{tot}, of 1 bar, a temperature of 1300°C, and oxygen fugacities in the range ~IW-10 to ~IW-1. In the following sections, we evaluate our data and discuss possible volatilization mechanisms in each of these distinct fO_2 regimes. We then consider implications for the survival of presolar grains of SiC in the solar nebula.

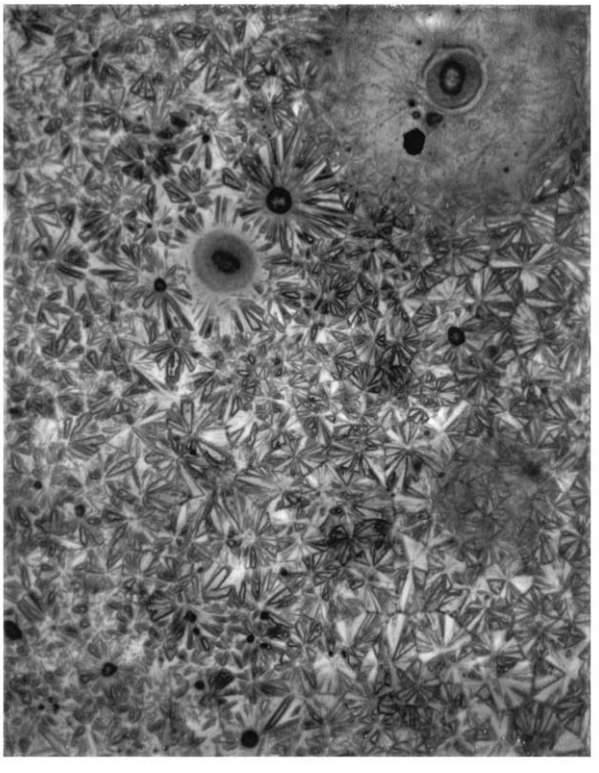

Fig. 14. Optical photomicrograph of the surface of a silica wafer (SiO_2 #QG-1) taken after exposure to H_2-CO_2 with log fO_2 = IW-6.0 at 1200 and 1300°C (total exposure time of 37 h). Field of view: 1.4 × 1.1 mm.

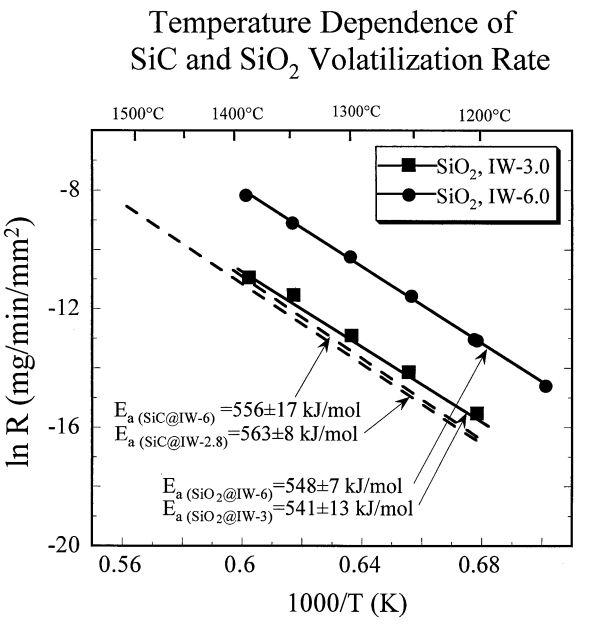

Fig. 15. Temperature dependence of SiO_2 volatilization rate in H_2-CO_2 at IW-3.0 (squares) and IW-6.0 (circles). SiC volatilization rates at IW-2.8 and IW-6.0 (dashed lines; cf. Fig. 8) are shown for comparison.

4.1. Volatilization in H_2-CO_2 above IW-3, Regime I

In this regime, SiC oxidation exhibits paralinear behavior ("c" in Fig. 4), caused by simultaneous formation and volatilization of a relatively thick cristobalite layer (Opila and Jacobson, 1995). The continuous silica layer seen on the surface of SiC exposed to H_2-CO_2 at IW-2.8 (e.g., Fig. 6) has two interfaces associated with it: an internal (SiC/SiO_2) one and an external (SiO_2/gas) one. Weight loss of SiC wafers might be

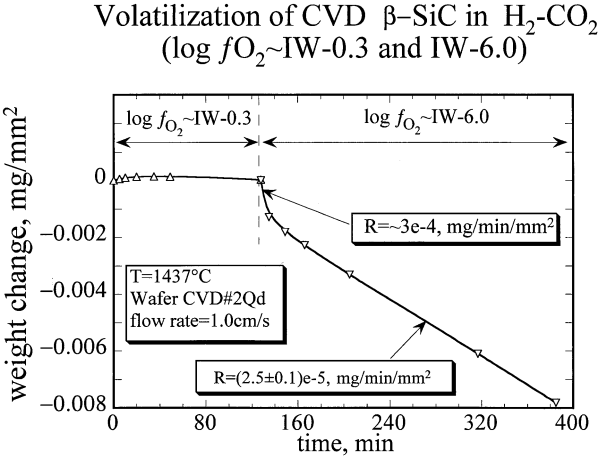

Fig. 16. Effect of preoxidation of β-SiC (CVD #2Qd) at IW-0.3 on weight loss rate at IW-6.0.

caused by solid–solid reactions, such as reaction 7, at the internal interface and/or by solid–gas reactions, such as reaction 8, at the external interface. Weight loss of SiO_2 wafers occurs only via reactions at the external interface, and its rate is expected and observed to be sensitive to gas composition. The near-equivalence of rates for SiC and silica glass in H_2-CO_2 suggests that any solid–solid reaction at the internal interface has a very small effect, if any, on the weight loss of SiC. This is probably due to a relatively thick surface silica layer on SiC that limits the supply of gases to and their removal from the internal interface, essentially shutting down possible reactions there. Furthermore, the volatilization rates of SiC and SiO_2 have the same fO_2 dependences and activation energies (Figs. 12 and 15). Taken together, our observations suggest that the weight loss rate of SiC in H_2-CO_2 above IW-3 is determined by a reaction at the external SiO_2/gas interface, such as reaction 8. The fact SiO_2 did not lose weight in CO-CO_2 at IW-1 (Table 3) suggests that the external interface is inert to gaseous carbon-bearing species under these conditions. As the thickness of the silica layer decreases due to its volatilization, the diffusion time of oxidizing species to the internal SiC/SiO_2 interface decreases, and the silica layer is replenished by passive oxidation of SiC via reactions such as reactions 1 to 3 or

$$SiC_{(s)} + 2H_2O_{(g)} \rightarrow SiO_{2(s)} + C_{(s)} + 2H_{2(g)}, \quad (9)$$

depending on the partial pressures of oxidizing species at the SiC/SiO_2 interface. These two competing processes (formation and volatilization of SiO_2) result in a roughly time invariant (steady state) thickness for the surface layer and a linear reaction rate. The slightly lower rate for SiC than for SiO_2, if real, could reflect the fact that SiC volatilization under these conditions involves both growth and volatilization of a silica layer.

4.2. Volatilization of SiC from IW-3 to IW-6: Role of Self-Buffering and Surface Coverage, Regime II

Figure 12 shows that although weight loss rates of SiC and SiO_2 in H_2-CO_2 gas mixtures at 1300°C have the same trend above IW-3, under more reducing conditions, the weight loss rates diverge. As fO_2 decreases, the rate for SiO_2 continues to increase, whereas that for SiC is essentially independent of fO_2 between ~IW-3 and ~IW-6. As a result, at IW-6, the SiO_2 volatilization rate is consistent with a linear extrapolation of the silica weight loss rate vs. log fO_2 trend from IW-1 to IW-3, and that for SiC is significantly lower. Thus, there must be a change in mechanism for SiC volatilization near IW-3. The same relationship between volatilization rate of SiC and partial pressure is observed regardless of which oxygen-bearing species (e.g., O_2, CO_2, H_2O) is plotted in Figure 12.

Figure 12, in combination with Figure 2a, shows that the weight loss rate of SiC in regime II remains constant despite large variations in partial pressures of major oxygen-bearing gaseous species. For example, at 1300°C, P_{CO} and P_{H_2O} decrease from 4×10^{-2} to 1×10^{-3} bars and P_{CO_2} decreases from 5×10^{-4} to 3×10^{-7} bars when fO_2 changes from 2×10^{-14} (IW-2.8) to 2×10^{-17} (IW-6). Moreover, SiC weight loss rates in CO-CO_2 remain essentially the same as in H_2-CO_2 at IW-6 and IW-2.8 (Fig. 8). These results show that volatilization of SiC in regime II is self-buffered, i.e., it occurs via a reaction that is independent of the external gas composition, probably through a reaction at the internal SiC/SiO_2 interface. One possibility is that a thin layer of silica protects the underlying SiC from direct contact with the gas phase and causes the reaction rate to be essentially independent of gas composition. A layer of silica is demonstrably present on SiC wafers run at IW-2.8, and our thermodynamic calculations (Fig. 2b) suggest that SiO_2 is stable at log $fO_2 >$ IW-5.5. Our TEM and RBS investigations of SiC wafers run at IW-6 show, however, that either no silica layer exists on the surface or that its thickness is less than 10 nm. Either a very thin (<10 nm) layer is in fact present at IW-6 or IW-6 is just slightly more reducing than necessary to generate such a layer.

If internal interface controlled reaction is responsible for weight loss in regime II, the transition from regime I (external interface controlled) to regime II is probably caused by a decrease in the thickness of the silica layer on SiC, due to the higher volatilization rate of SiO_2 under more reducing conditions. Thinning of the layer decreases the supply, the removal time, or both of gaseous species through the layer to or from the SiC/SiO_2 interface, which could change the rate-limiting step in such a way that the rate of chemical reaction at the internal interface becomes dominant in the overall SiC volatilization. It is unclear which solid–solid reaction is responsible for weight loss of SiC in regime II. One possibility is that the interface reaction in regime I is incomplete oxidation via a reaction such as reaction 9. Perhaps thinning of the silica layer results in a higher delivery rate of oxidants to the SiC surface in regime II, allowing complete oxidation of SiC via reactions 1 to 3. On the other hand, partial pressures of oxidizing species in the gas mixtures are lower in regime II than in regime I. Perhaps the fluxes of oxidants to the SiC surface are lower in regime II, leading to incomplete oxidation with formation of elemental carbon in regime II. RBS and TEM characterization of samples run at different fO_2s could resolve this issue.

Our RBS data at IW-2.8 show that carbon is present at the oxide–carbide interface (Fig. 6b). In this case, the weight loss could conceivably occur due to reaction 7 via the mechanism proposed by Jacobson et al. (1992), or due to

$$SiO_{2(s)} + C_{(s)} \rightarrow SiO_{(g)} + CO_{(g)}. \quad (10)$$

In both cases, calculated P_{CO} and P_{SiO} at the internal (SiC/SiO_2/C) interface are significantly higher than those at the external solid/gas interface, causing SiO and CO to diffuse outward from the internal interface. Because the thickness of the cristobalite layer is very small (significantly less than 1 μm), reaction products can easily diffuse through it (Zheng et al., 1990) or along grain boundaries. Regardless of whether SiC volatilization in regime II occurs via reaction 7 or 10, the rate should be independent of gas composition, as observed in our experiments.

Other workers have also observed ranges of redox conditions over which the reaction rate is essentially constant, and possible mechanisms of SiC weight loss and arguments in favor of or against each one are presented in Table 4. For example, Kim (1987) and Kim and Readey (1989) found, as mentioned earlier, that in H_2-H_2O gas mixtures the SiC weight loss rate at 1400°C is nearly constant between IW-4.6 and IW-7.4. At lower temperatures, this range expands to even lower oxygen fugacities. Following Turkdogan et al. (1963), Kim (1987)

Table 4. Possible weight loss mechanisms in regime II.

Possible mechanism	Effect of gas composition	Gas flow rate dependence	Activation energy	Issues
1. Solid–solid reaction interfacial reactions: a) $2SiO_{2(s)} + SiC_{(s)} \rightarrow 3SiO_{(g)} + CO_{(g)}$,	Independence of weight loss rate from composition of flowing gas is expected—observed.	Weight loss rate is expected to be independent of gas flow rates—observed (at least between 0.5 and 1.6 cm/s).	Measured E_a (~560 kJ/mol) is essentially the same as expected for 1a (548 kJ/mol).	Why is SiO_2 not volatilized when on SiC, but attacked when alone?
b) $SiO_{2(s)} + C_{(s)} \rightarrow SiO_{(g)} + CO_{(g)}$.				
2. Smoke formation: a) $SiO_{2(s)} + H_{2(g)} \rightarrow SiO_{(g)} + H_2O_{(g)}$	Weight loss rate is expected to be dependent on gas composition—not observed.	$V^{0.5}$ dependency is expected—not observed.		Redeposition of SiO_2 whiskers is expected on wafer surfaces—not observed.
or b) $2SiO + SiC_{(s)} \rightarrow 3SiO_{(g)} + CO_{(g)}$, followed by c) $SiO_{(g)} + 1/2\ O_{2(g)} \rightarrow SiO_{2(s)}$				
3. Volatilization of discontinuous oxide layer from the surface of SiC: $SiO_{2(s)} + H_{2(g)} \rightarrow SiO_{(g)} + H_2O_{(g)}$	Same as for 2.	Same as for 2.	E_a (540–560 kJ/mol) is essentially the same as measured.	Surface area of oxide must decrease by exactly the amount needed to offset the increase in the volatilization rate as the gas becomes more reducing.
4. SiO_2 formation is rate limiting	Same as for 2.	Same as for 2.	Low E_a (<300 kJ/mol) under most conditions—not observed.	

proposed that silica fumes (clouds of tiny grains of SiO_2) form above the surface of SiC by oxidation of $SiO_{(g)}$, and that these fumes buffer the gas composition between the fumes and the surface. Another explanation (e.g., Antill and Warburton, 1971; Kim and Readey, 1989) involves formation of a discontinuous silica layer on the surface of SiC. In order for the volatilization rate to remain independent of fO_2, the surface area of SiO_2 must decrease with decreasing fO_2 by precisely the amount needed to compensate for the concomitant increase in the volatilization rate of SiO_2. Although we are skeptical of both of these explanations, we cannot rule out either of them.

4.3. Volatilization of SiC below IW-6, Regime III

At oxygen fugacities more reducing than IW-6 (regime III in Figure 12), the weight loss rate of SiC increases with decreasing fO_2 in our experiments. Our interpretation is that under such reducing conditions, the very limited supply of oxidants does not allow formation of a continuous silica layer, and the weight loss occurs via a combination of active oxidation of bare SiC and volatilization of SiO_2 remaining inside pits and along grain boundaries. With decreasing fO_2, the rate is expected to reach a maximum at some $fO_2 <$ IW-10 (fO_2^{trans}, not shown), and then decrease in accord with true active oxidation of bare SiC via reactions 4 to 6 (Rosner and Allendorf, 1970; Kim, 1987; Narushima et al., 1997; Schneider et al., 1998). In the vicinity of fO_2^{trans}, there appear to be at least three major processes taking place: active oxidation of SiC from bare surfaces, formation of SiO_2 on the surface, and volatilization of the SiO_2 (e.g., Rosner and Allendorf, 1970; Schneider et al., 1998). When fO_2^{trans} is approached from the reducing side, silica forms inside pits and along grain boundaries (e.g., Kim and Moorhead, 1990) via reactions 1 to 3, and decreases the surface area of bare SiC, leading to a decrease in the contribution of active oxidation to the overall volatilization rate. If the rate of silica formation in this regime is greater than the rate of active oxidation of SiC but lower than the silica evaporation rate (e.g., reaction 8), the wafer will continue to lose weight. Because the weight loss rate of silica decreases as the gas becomes more oxidizing, as discussed earlier, this results in a decrease in the overall rate of SiC volatilization, as observed in Figure 12. As the fO_2 is increased above ~IW-6, a continuous layer of silica exists on the surface of SiC and the volatilization mechanism changes, as described above (section 4.2).

4.4. Survival of Presolar SiC Grains in the Solar Nebula

The main goal of this study is to use the results of experiments on the volatilization of synthetic SiC to place constraints on the nature of nebular environments to which meteoritic SiC could have been exposed. The abundance of SiC found as large, in situ matrix grains in Murchison is roughly consistent with bulk values (Alexander et al., 1990), probably indicating that most presolar SiC occurs in the low-temperature, matrix component of the chondrites. Investigation of SiC grains isolated from Murchison with a nonerosive, acid-free disaggregation method (Macke et al., 1999) showed that they have very irregular surfaces, and that silica is abundant on the surface of SiC grains (as a layer a few nanometers thick). This indicates that at least some SiC grains experienced chemical interaction with a nebular gas or with fluids in the parent body that led to

the production of silica. Perhaps more importantly, it also suggests that a thin silica film may have been involved in the volatilization of presolar SiC and that therefore, volatilization rates from the present study for oxygen fugacities above IW-6 could be used for constraining the lifetimes of presolar SiC grains.

The partial pressures of major gaseous species in the H_2-CO_2 and CO-CO_2 gas mixtures (log fO_2 from IW-10 to IW+1) used in our experiments were in the range 1×10^{-6} to 1 atm for H_2, 1×10^{-6} to 5×10^{-2} atm for H_2O, $\sim 2 \times 10^{-6}$ to 1 atm for CO, and $\sim 10^{-11}$ to 5×10^{-4} atm for CO_2. These values bracket those of O_2, H_2, and CO_2 expected in a gas of solar composition (log fO_2 = IW-6) and approach those of H_2O and CO (Lewis and Prinn, 1980; Sharp and Huebner, 1990). The similar partial pressures for the gaseous species most likely to play a major role in the reactions by which SiC is consumed make it plausible that the steps involved in the volatilization of presolar SiC grains under solar nebular conditions were similar to those in our experiments. Thus, for example, if silica on the surface of presolar SiC grains (Macke et al., 1999) was formed in the solar nebula, and volatilization of SiC was controlled by the solid–solid chemical reaction 7 at an SiC/SiO_2 interface, then a change in the total pressure in the system and modest differences in the composition of the gas phase would not be expected to significantly affect the volatilization rate. The lifetimes of SiC grains can, under this assumption, be calculated by the relationship

$$dm = RSdt = d(V\rho) \quad (11)$$

together with our experimentally determined reaction rates. In Eqn. 11, m, R, S, t, V, and ρ are the weight, reaction rate, surface area, time, volume, and density (ρ_{SiC} = 3.2 g/cm^3). For spherical grains, Eqn. 11 reduces to

$$dt = \rho da/2R, \quad (12)$$

where a is the diameter. According to size distributions in the Murchison carbonaceous chondrite (Amari et al., 1994), almost all meteoritic SiC grains are less than 10 μm in diameter, and the average is less than 1 μm. Assuming that our experimentally determined SiC weight loss rates at IW-6.0, the redox conditions corresponding to a gas of solar composition, are appropriate, integration of Eqn. 12 for a 1-μm-diameter SiC grain indicates that it could survive in the solar nebula for $\sim$1 h at 1400°C, $\sim$1 d at 1300°C, $\sim$1 yr at 1100°C, and several thousand years at $\sim$900°C, as shown in Figure 17. SiC grains 10 μm in diameter would survive at these temperatures for an order of magnitude longer, but this is still a much shorter period of time than the lifetime or cooling time of the hot, inner regions of the solar nebula, $\sim 10^4$ to 10^7 yr (Clark et al., 1972; Tscharnuter and Boss, 1993). Only at temperatures below $\sim$870°C (1 μm diameter) and $\sim$930°C (10 μm diameter) are calculated lifetimes of SiC grains comparable to estimated lower limits on the cooling times for the solar nebula ($>10^4$ yr). The lifetimes estimated above are based on our experimental results obtained at gas flow rates >0.5 cm/s. Cameron (1995) estimated that radial drift velocities of 10-μm grains in the inner solar nebula (1 to 5 AU) were $\sim$0.03 to 0.05 cm/s. Kim (1987) and Kim and Readey (1989) observed that the SiC volatilization rate decreases by a factor of two when gas flow

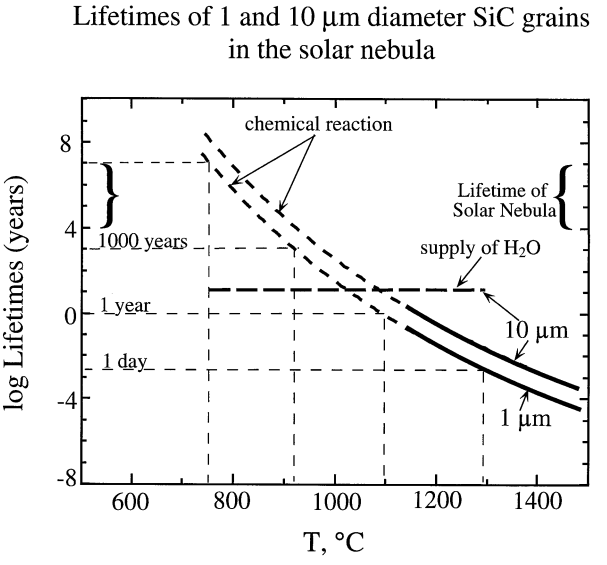

Fig. 17. Temperature dependence of lifetimes in a solar gas (log fO_2 = IW-6) for 1- and 10-μm-diameter presolar SiC grains when volatilization is controlled by chemical reactions at the SiC/SiO_2 interface. These curves are labeled "chemical reaction" and are solid where calculated directly from our experimental data and dashed where extrapolated. The line labeled "supply of H_2O" is the conversion time of a 10-μm-diameter SiC grain to SiO_2 calculated from the supply rate of $H_2O_{(g)}$ for $P^{tot} = 10^{-6}$ atm and α = 0.01. Curly brackets, denoting the duration of the hot nebular stage (Clark et al., 1972; Tscharnuter and Boss, 1993), are shown for comparison.

rate decreases by a factor of 5 above 1400°C in H_2-H_2O gas mixtures with $P_{H_2O} \leq 10^{-3}$ atm. If we assume a similar relationship between the SiC volatilization rate and flow rate in a gas of solar composition, the SiC volatilization rates in the solar nebula would have been about a factor of three lower than our experimental values. Such a small decrease in volatilization rate would not dramatically affect the lifetimes of SiC grains presented above. According to current solar nebula models (Cassen, 1994, 2001; Boss, 1998), maximum temperatures higher than 1000°C could be maintained in the midplane of the solar nebula inside 2 AU for 10^5 to 10^6 yr, but they fall sharply to <0°C outside $\sim$5 AU. Our results on SiC volatilization suggest that although presolar SiC grains could potentially survive short heating events such as those associated with formation of chondrules (minutes) and melting of calcium-, aluminum-rich inclusions (CAIs) (days), the grains could not have remained in the hot inner portion (<2 AU) of the solar nebula for an extended period of time without being destroyed. It is possible that some SiC grains did in fact survive such a thermal treatment as inclusions in high temperature minerals, but the similarity of bulk and matrix concentrations of SiC (Alexander et al., 1990) suggests that armoring of this type was not a major survival mechanism for SiC.

The nebular lifetimes for SiC grains discussed above were obtained assuming that the grains are covered by a thin layer of silica and that the SiC volatilization rate is controlled by the reaction rate at SiC/SiO_2 interfaces, allowing us to use our experimentally determined weight loss rates. At the low total pressures relevant to the solar nebula, 10^{-3} to 10^{-6} atm (Wood and Morfill, 1988; Tscharnuter and Boss, 1993; Cassen, 1994;

Boss, 1998), however, partial pressures of oxidizing species are so low that formation of a silica layer on SiC surfaces may be impeded. In this case, the supply rate of oxidants to the surface of SiC may have been too low to produce SiO_2 at a rate sufficient to sustain the solid–solid reaction at the experimentally measured volatilization rate. In other words, the supply of oxidants to the surface may have been rate limiting. This issue can be explored by the Hertz-Knudsen equation (Knudsen, 1909), which expresses the flux of a gaseous species *i* as

$$J_i = \alpha \frac{P_i}{(2\pi M_i R_o T)^{1/2}}, \quad (13)$$

where α is the sticking coefficient, M_i and P_i are the molecular weight and partial pressure of the oxidant, and R_o is the gas constant. H_2O, the second most abundant O-bearing species in the nebular vapor at high temperatures (>700°C), is the most likely oxidant because CO and SiO, the alternatives with relatively high partial pressures, are too thermodynamically stable to be reduced into elemental C or Si in a gas of solar composition. Because P_{H_2O} is proportional to total pressure, P^{tot}, in H-rich nebular gases of constant bulk composition at low P^{tot}, fluxes calculated from Eqn. 13 are also proportional to P^{tot}. If α is defined as the fraction of H_2O molecules striking the surface of a grain that actually react with it, then J_{H_2O} is also the conversion rate of surface SiC to SiO_2 (i.e., the rate of formation of the silica layer). If solar nebular conditions were such that J_{H_2O} was very small relative to our experimentally determined volatilization rate, the overall SiC volatilization rate would have been controlled by the supply of $H_2O_{(g)}$, and the volatilization rate would have been equal to J_{H_2O}. The value of α for SiC in a nebular gas is unknown but it can be no higher than 1.0 and is probably no lower than 0.01, the lowest value in the compilation of Kaneko et al. (1996) for gas molecules striking SiC. At the high end of plausible values for sticking coefficient (1.0) and P^{tot} (10^{-3} atm), the SiC conversion rates calculated by Eqn. 13, $\sim 1.5 \times 10^{-6}$ mol/min/mm^2, are higher than experimentally determined SiC volatilization rates, 1.2×10^{-9} and 0.4×10^{-6} mol/min/mm^2 at 1200 and 1400°C, respectively. Under these conditions, therefore, the SiC conversion rate, and hence the supply of oxidants is probably not rate limiting for the overall reaction. On the other hand, at the low end of values for α (0.01) and P^{tot} (10^{-6} atm), the effective flux of $H_2O_{(g)}$ to SiC surfaces would be too low by a factor of ~20 at 1200°C and ~5000 at 1400°C to produce SiO_2 at a rate capable of sustaining the experimentally observed weight loss rates. Because extrapolation of our experimental results to lower temperatures yields much lower volatilization rates, however, calculated H_2O fluxes would be more than sufficient to sustain the SiC/SiO_2 interface reaction below ~1100°C at 10^{-6} atm and $\alpha = 0.01$.

The curves labeled "chemical reaction" in Figure 17 are calculated lifetimes as a function of temperature for 1- and 10-μm-diameter SiC grains by using our experimentally determined volatilization rates. Also shown (as the dashed line) is the lifetime of a 10-μm-diameter SiC grain if its volatilization rate is controlled by supply of $H_2O_{(g)}$, the rate of which was calculated by using the extreme case of $P^{tot} = 10^{-6}$ atm and $\alpha = 0.01$ in Eqn. 13. It is seen that if chemical reaction is the rate-limiting step, the lifetime of SiC grains increases as temperature decreases, such that a 10-μm SiC grain would survive 10^4 yr at ~870°C, or 10^7 yr at ~750°C. If instead the supply of H_2O to the surface of SiC is the rate-limiting step, the lifetime is relatively insensitive to temperature and would be ~10 yr for 10-μm SiC grains and ~1 yr for 1-μm grains within the temperature range 750 to 1300°C. For 10-μm grains, the 10-yr lifetime is shorter than lifetimes calculated from our experimental data for temperatures below 1100°C, where we thus conclude that the lifetime of SiC grains is determined by the rate of chemical reaction. Above 1100°C, the lifetime of SiC grains is determined by the supply rate of oxidant, J_{H_2O}, and thus by the conversion rate of surface SiC to silica. The conversion time shifts downward by one log unit for every order of magnitude increase in either P^{tot} or α, increasing the temperature of intersection of the conversion time line with the curve of lifetimes based on our experimental data. This in turn increases the maximum temperature at which oxidant supply is sufficient to sustain the interface reaction.

Rubin et al. (1988) pointed out that formation of some components of chondrites requires the log fO_2 of the nebular gas to be higher than IW-6, whereas others require it to be lower than this value. On the basis of the fO_2 dependence of the SiC weight loss rate (Fig. 12) and assuming that the volatilization mechanism in the solar nebula is the same as in our experiments, we expect that if the nebular fO_2 were more reducing than a gas of solar composition, calculated SiC lifetimes would be even shorter than estimated above. If the fO_2 of the nebular gas were up to three log units more oxidizing than a gas of solar composition, then calculated lifetimes of presolar SiC grains would be essentially the same as estimated above. If the solar gas were as oxidizing as IW-1 (i.e., ~5 log units more oxidizing than a gas of solar composition), the calculated lifetimes based on our experiments are higher by about a factor of five, but this would still be ~10^2 to 10^5 times shorter than the duration of the high temperature stage (>1000°C, ~10^5 to 10^6 yr) in the inner part of the solar nebula.

The effect of changing redox conditions on reaction rates controlled by oxidant supply scales with the partial pressure of H_2O. For a constant total pressure, increasing the O/H ratio of a gas that is otherwise solar in composition such that the nebular fO_2 increases from IW-6 to ~IW-2 generates an ~30-fold increase in the partial pressure of H_2O. This would lead to a corresponding ~30-fold increase in the flux of H_2O to the surface of SiC grains and, if H_2O supply is the rate-limiting step, to a ~30-fold decrease in SiC lifetimes. However, increasing the partial pressure of H_2O also increases the temperature above which H_2O supply is rate limiting. For gas compositions more reducing than IW-6, where the volatilization mechanism is active oxidation, reactions 4 to 6, the reaction rate again scales with the supply of oxidant to the surface of the SiC. Decreasing the fO_2 from IW-6 to ~IW-10 would yield a decrease in the partial pressure and flux of H_2O by a factor of ~30, resulting in an increase in the lifetime of presolar SiC grains to tens of years and hundreds of years for 1- and 10-μm-diameter grains, respectively, at $P^{tot} = 10^{-6}$ atm.

Passage through the accretion front can be a highly energetic process, potentially capable of destroying interstellar grains as they enter the solar nebula. Model calculations (e.g., Cassen and Chick, 1997) show that although presolar grains remain

cold (less than −100°C) during their passage through the accretion front at a heliocentric distance of >10 AU, they heat up to ~750°C at 1 AU, and to even higher temperatures at distances closer to the protosun. Because the deceleration distances for small grains (<10 μm diameter) are less than the 10^4- to 10^5-km thickness of the accretion front and the shock wave velocity is ~10 to 100 km/s (Cassen and Chick, 1997), the duration of heating for presolar SiC would have been less than several hours. Even if oxidant supply is not rate limiting, such short timescales could only result in destruction of 1- to 10-μm-diameter grains if the peak temperature exceeded 1400°C (Fig. 17), and such conditions would only be expected very close to the protosun. We conclude that interstellar SiC grains would not have been strongly affected by passage through the accretion front of the solar nebula outside 1 AU.

After interstellar SiC grains are accreted into the solar nebula, they are essentially coupled to the gas phase due to their small size (e.g., Weidenschilling, 1977; Cameron, 1995). Although gas parcels in the vicinity of 3 AU would carry such small particles inward under most circumstances, Cassen (2001) also illustrated conditions where parcels gain angular momentum and carry such small particles as far as ~0.1 AU outward into cooler regions on a timescale of $\sim 5 \times 10^3$ yr. From theoretical estimates of nebular midplane temperature gradients (Cassen, 1994; Boss, 1998), these transport distances are capable of cooling the grains only by <100°C. Thus, this process could only lead to survival of those grains that originally resided in regions whose temperatures were already low enough (~900°C) to ensure their survival for several thousand years.

Experimental data indicate that temperatures in the solar nebula reached 1550 to 1900°C and 1400°C during melting of chondrule (Hewins, 1997) and CAI (Stolper and Paque, 1986) precursors, respectively. At these temperatures, nebular lifetimes of 10-μm SiC grains controlled by oxidant supply are more than 10 yr. SiC grains were thus able to survive the minute-long flash heating events associated with chondrule formation as envisioned by Hewins and Connolly (1996) and the several day-long freezing times of CAIs envisioned by MacPherson et al. (1984), provided the SiC grains were not inside the chondrules or CAIs themselves where they would have been subject to dissolution into silicate melt, the rate of which is not constrained by our experiments.

On the basis of the small amount of SiC relative to diamond in the matrices of CV and CO chondrites compared to EH chondrites, Huss and Lewis (1995) and Huss (1997) concluded that SiC was volatilized at 600 to 650°C before accretion of the CV and CO chondrites. The results shown on Figure 17 would seem to imply prohibitively long SiC lifetimes at these temperatures for this model to be correct. It should be noted, however, that our results are based on experimental data obtained at relatively high temperatures, and they cannot be simply extrapolated to temperatures as low as 600°C without demonstration that the volatilization mechanism, and the temperature and composition dependences remain the same as at the experimental conditions.

5. SUMMARY AND CONCLUSIONS

We determined the volatilization kinetics of SiC (α and β) and SiO_2 (glass) in H_2-CO_2, CO-CO_2 and H_2-CO-CO_2 gas mixtures at log fO_2 values from IW+1.0 to IW-10.4 and temperatures in the range 1151 to 1501°C. Detailed sets of experiments were conducted at IW-2.8 and IW-6.0 as a function of temperature, and at 1300°C as a function of fO_2. Under oxidizing conditions (log fO_2 > IW-3), the weight loss rate of SiC is controlled by the volatilization rate of silica, which forms a thin layer on the surface of the SiC. For oxygen fugacities in the range ~IW-3 to ~IW-6, the rate of weight loss for SiC is independent of externally imposed concentrations of O-bearing species, which suggests that the SiC volatilization is self-buffered, most likely by a thin surface layer of silica that partially protects SiC from the surrounding gas. Weight loss of SiC is probably controlled by a solid–solid reaction at the oxide–carbide interface. Activation energies for volatilization of SiC are 563 ± 8 kJ/mol at IW-2.8 and 556 ± 17 kJ/mol at IW-6.0. Under more reducing conditions (log fO_2 < ~IW-6), SiC weight loss occurs via a combination of true active oxidation of bare SiC surfaces and volatilization of SiO_2 from inside pits and along incised SiC grain boundaries.

If the rate of SiC volatilization in the solar nebula were the same as in our experiments in H_2-CO_2 gas mixtures at IW-6, then the estimated lifetime of a 1-μm-diameter presolar SiC grain ranges from several thousand years at 900°C, to ~1 yr at 1100°C, ~1 d at 1300°C, and ~1 h at 1400°C, independent of P^{tot}. The lifetimes of 10-μm SiC grains are longer by an order of magnitude. Because of the relatively low P^{tot} of the solar nebula, however, supply of $H_2O_{(g)}$ to surfaces of presolar SiC was probably rate limiting at very high temperatures. Under these circumstances, calculated lifetimes of SiC grains would be 1 yr for 1-μm-diameter and 10 yr for 10-μm-diameter grains above 1100°C at $P^{tot} = 10^{-6}$ atm, for example.

We have seen that the lifetimes of SiC grains in nebular gases at or above 900°C are short compared to theoretical estimates of the cooling times of hot nebular regions and compared to estimates of grain travel times from hot to cool regions in the equatorial plane of the disk. Thus, although presolar SiC grains could survive short heating events associated with formation of chondrules (minutes) and melting of CAIs (days), those presolar SiC grains that survived the nebular stage were not exposed to hot (≥900°C) nebular gas for more than several thousand years, either because they accreted to the cool, outer parts of the solar nebula or to the inner part but only after it had cooled below ~900°C. Alternatively, it is conceivable that survival of presolar SiC grains for longer times and/or at higher temperatures was assisted by their being encased in grains of minerals that were inert to reaction with solar nebular gas.

Acknowledgments—We are grateful to J. Goela, M. Pickering, and R. Taylor for providing us with CVD β-SiC; we thank P. Laurijsen and H. Kolker for single-crystal α-SiC. We thank Joe Pluth for his help with XRD and P. Cassen for insights into nebular dynamics. Avi Zangvil and Senol Pekin participated in useful discussions. Reviews by G. Huss, K. Lodders, N. Jacobson, and E. Opila greatly improved the manuscript. This work was supported by the National Aeronautics and Space Administration through grants NAGW-3212 (L.G.), NAG5-4476 (L.G.), NAG5-4318 (E.S.), and NAG5-6184 (E.S.). R.A.M.'s

participation in the late stages of this study was made possible with funds from NASA grant NAG5-9378 to Frank M. Richter.

Associate editor: U. Ott

REFERENCES

Alexander C. M. O'D., Swan P., and Walker R. M. (1990) In situ measurement of interstellar silicon carbide in two CM chondrite meteorites. *Nature* **348,** 715–717.

Amari S., Lewis R. S., and Anders E. (1994) Interstellar grains in meteorites: I. Isolation of SiC, graphite, and diamond; size distributions of SiC and graphite. *Geochim. Cosmochim. Acta* **58,** 459–470.

Amari S. and Zinner E. (1997) Supernova grains from meteorites. In *Astrophysical Implications of the Laboratory Study of Presolar Materials; AIP Conference Proceedings 402* (eds. T. J. Bernatowicz and E. Zinner), pp. 287–305. American Institute of Physics.

Anders E. and Zinner E. (1993) Interstellar grains in primitive meteorites: Diamond, silicon carbide, and graphite. *Meteoritics* **28,** 490–514.

Antill J. E. and Warburton J. B. (1971) Active to passive transition in the oxidation of SiC. *Corr. Sci.* **11,** 337–342.

Barin I. (1989) *Thermochemical Data of Pure Substances.*VCH.

Bauer J., Fiala J., and Hrichová R. (1963) Natural α-silicon carbide. *Am. Mineral.* **48,** 620–634.

Beckett J. R. and Mendybaev R. A. (1997) The measurement of oxygen fugacities in flowing gas mixtures at temperatures below 1200°C. *Geochim. Cosmochim. Acta* **61,** 4331–4336.

Bernatowicz T., Fraundorf G., Tang M., Anders E., Wopenka B., Zinner E., and Fraundorf P. (1987) Evidence for interstellar SiC in the Murray carbonaceous meteorite. *Nature* **330,** 728–730.

Bird R. B., Stewart W. E., and Lightfoot E. N. (1960) *Transport Phenomena.* Wiley.

Boss A. P. (1998) Temperatures in protoplanetary disks. *Ann. Rev. Earth Planet. Sci.* **26,** 53–80.

Bravman J. C. and Sinclair R. (1984) The preparation of cross-section specimens for transmission electron microscopy. *J. Electron Micros. Techn.* **1,** 53–61.

Butt D. P., Tressler R. E., and Spear K. E. (1992) Corrosion of SiC materials in N_2-H_2-CO gaseous environments: I, Thermodynamics and kinetics of reactions. *J. Am. Ceramic Soc.* **75,** 3257–3267.

Cameron A. G. W. (1995) The first ten million years in the solar nebula. *Meteoritics* **30,** 133–161.

Cassen P. (1994) Utilitarian models of the solar nebula. *Icarus* **112,** 405–429.

Cassen P. (2001) Nebular thermal evolution and the properties of primitive planetary materials. *Meteorit. Planet. Sci.* **36,** 671–700.

Cassen P. and Chick K. M. (1997) The survival of presolar grains during the formation of the solar system. In *Astrophysical Implications of the Laboratory Study of Presolar Materials; AIP Conference Proceedings 402* (eds. T. J. Bernatowicz and E. Zinner), pp. 697–719. American Institute of Physics.

Chase M. W. Jr., Davies C. A., Downey J. R. Jr., Frurip D. J., McDonald R. A., and Syverud A. N. (1985) *JANAF Thermochemical Tables,*3rd ed. *J. Phys. Chem. Ref. Data.* Vol. **14,** Suppl. 1.

Chu W.-K., Mayer J. W., and Nicolet M.-A. (1978) *Backscattering Spectroscopy.*Academic Press.

Clark S. P. Jr., Turekian K. K., and Grossman L. (1972) Model for the early history of the earth. In *Nature of the Solid Earth* (ed. E. C. Robertson), pp. 3–18. McGraw-Hill.

Cooper R. F. and Chyung K. (1987) Structure and chemistry of fibre-matrix interfaces in silicon carbide fibre-reinforced glass-ceramic composites: An electron microscopy study. *J. Mater. Sci.* **22,** 3148–3160.

Cooper R. F., Fanselow J. B., and Poker D. B. (1996) The mechanism of oxidation of a basaltic glass: Chemical diffusion of network-modifying cations. *Geochim. Cosmochim. Acta* **60,** 3253–3265.

Costello J. A. and Tressler R. E. (1981) Oxidation kinetics of hot-pressed and sintered α-SiC. *J. Am. Ceramic Soc.* **64,** 327–331.

Davis A. M. and MacPherson G. J. (1996) Thermal processing in the solar nebula: Constraints from refractory inclusions. In *Chondrules and the Protoplanetary Disk* (eds. R. H. Hewins, R. H. Jones, and E. R. D. Scott), pp. 71–76. Cambridge University Press.

Doolittle L. R. (1985) Algorithms for the rapid simulation of Rutherford backscattering spectra. *Nucl. Instr. Methods Phys. Res.* **B9**, 344–351.

Ervin G. J. (1958) Oxidation behavior of silicon carbide. *J. Am. Ceramic Soc.* **41,** 347–352.

Fegley B. Jr. (1988) Cosmochemical trends of volatile elements in the solar system. In *Workshop on the Origins of Solar Systems* (ed. J. A. Nuth and P. Sylvester), pp. 51–60. LPI Technical Report 88-04, Lunar and Planetary Institute.

Filippidis A. (1993) New find of moissanite in the Metaxades zeolite-bearing volcaniclastic rocks, Thrace County, Greece. *N. Jb. Mineral. Mon.* (ll):521–527.

Gardner R. A. (1974) The kinetics of silica reduction in hydrogen. *J. Solid State Chem.* **9,** 336–344.

Geankoplis C. J. (1972) *Mass Transport Phenomena.* Holt, Rinehart and Winston.

Grossman L. (1972) Condensation in the primitive solar nebula. *Geochim. Cosmochim. Acta* **36,** 597–619.

Gulbransen E. A., Andrew K. F., and Brassart F. A. (1966) The oxidation of silicon carbide at 1150°C to 1400°C and at 9×10^{-3} to 5×10^{-1} torr oxygen pressure. *J. Electrochem. Soc.* **113,** 1311–1314.

Gulbransen E. A. and Jansson S. A. (1972) The high-temperature oxidation, reduction, and volatilization reactions of silicon and silicon carbide. *Oxid. Metals* **4,** 181–201.

Hewins R. H. (1997) Chondrules. *Ann. Rev. Earth Planet. Sci.* **25,** 61–83.

Hewins R. H. and Connolly H. C. Jr. (1996) Peak temperatures of flash-melted chondrules. In *Chondrules and the Protoplanetary Disk* (eds. R. H. Hewins, R. H. Jones, and E. R. D. Scott), pp. 197–204. Cambridge University Press.

Hoppe P., Amari S., Zinner E., Ireland T., and Lewis R. S. (1994) Carbon, nitrogen, magnesium, silicon and titanium isotopic compositions of single interstellar silicon carbide grains from the Murchison carbonaceous chondrite. *Astrophys. J.* **430,** 870–890.

Hoppe P. and Ott U. (1997) Mainstream silicon carbide grains from meteorites. In *Astrophysical Implications of the Laboratory Study of Presolar Materials; AIP Conference Proceedings 402* (eds. T. J. Bernatowicz and E. Zinner), pp. 27–58. American Institute of Physics.

Huss G. R. (1997) The survival of presolar grains in solar system bodies. In *Astrophysical Implications of the Laboratory Study of Presolar Materials; AIP Conference Proceedings 402* (eds. T. J. Bernatowicz and E. Zinner), pp. 721–748. American Institute of Physics.

Huss G. R. and Lewis R. S. (1995) Presolar diamond, SiC, and graphite in primitive chondrites: Abundances as a function of meteorite class and petrologic type. *Geochim. Cosmochim. Acta* **59,** 115–160.

Huss G. R., Hutcheon I. D., and Wasserburg G. J. (1997) Isotopic systematics of presolar silicon carbide from the Orgueil (CI) chondrite: Implications for solar system formation and stellar nucleosynthesis. *Geochim. Cosmochim. Acta* **61,** 5117–5148.

Jacobson N. S. (1993) Corrosion of silicon-based ceramics in combustion environments. *J. Am. Ceramic Soc.* **76,** 3–28.

Jacobson N. S., Eckel A. J., Misra A. K., and Humphrey D. L. (1990) Reaction of SiC with H_2/H_2O/Ar mixtures at 1300°C. *J. Am. Ceramic Soc.* **73,** 2330–2332.

Jacobson N. S., Lee K. N., and Fox D. S. (1992) Reactions of silicon carbide and silicon (IV) oxide at elevated temperatures. *J. Am. Ceramic Soc.* **75,** 1603–1611.

Jorgensen P. J., Wadsworth M. E., and Cutler I. B. (1959) Oxidation of silicon carbide. *J. Am. Ceramic Soc.* **42,** 613–616.

Kaneko T., Sone H., Miyakawa N., and Naka M. (1996) Growth kinetics of various vapor-grown SiC. In *Silicon Carbide and Related Materials, 1995; IP Conference Series 142* (eds. S. Nakashima, H. Matsunami, S. Yoshida, and H. Harima), pp. 53–56. Institute of Physics Publishing.

Kim H.-E. (1987) Gaseous corrosion of silicon carbide and silicon nitride in hydrogen. Ph.D. dissertation. Ohio State University.

Kim H.-E. and Readey D. W. (1989) Active oxidation of SiC in low

dew-point hydrogen above 1400°C. In *Silicon Carbide '87* (eds. J. D. Cawley and C. E. Semier), pp. 301–312. American Ceramic Society.

Kim H.-E. and Moorhead A. J. (1990) Effect of hydrogen-water atmospheres on corrosion and flexural strength of sintered α-silicon carbide. *J. Am. Ceramic Soc.* **73,** 694–699.

Knudsen M. (1909) Die Molekularströmung der Gase durch Öffnungen und die Effusion. *Ann. Phys. 4th Ser.* **28**, 999–1016.

Larimer J. W. and Bartholomay M. (1979) The role of carbon and oxygen in cosmic gases: Some applications to the chemistry and mineralogy of enstatite chondrites. *Geochim. Cosmochim. Acta* **43,** 1455–1466.

Lattimer J. M. and Grossman L. (1978) Chemical condensation sequences in supernova ejecta. *Moon Planets* **19,** 169–184.

Leung I. S. (1990) Silicon carbide cluster entrapped in a diamond from Fuxian, China. *Am. Mineral.* **75,** 1110–1119.

Lewis J. S. and Prinn R. G. (1980) Kinetic inhibition of CO and N_2 reduction in the solar nebula. *Astrophys. J.* **238,** 357–364.

Lewis R. S., Amari S., and Anders E. (1994) Interstellar grains in meteorites: II. SiC and its noble gases. *Geochim. Cosmochim. Acta* **58,** 471–494.

Macke R. J., Bernatowicz T., Swan P., Walker R. M., and Zinner E. (1999) Non-chemical isolation of silica and presolar SiC from Murchison (abstract 1435). *Lunar Planet. Sci. Conf.* **XXX** (CD-ROM).

MacPherson G. J., Paque J. M., Stolper E., and Grossman L. (1984) The origin and significance of reverse zoning in melilite from Allende Type B inclusions. *J. Geol.* **92,** 289–305.

Marshintsev V. K., Zayakina N. B., and Leskova N. B. (1982) Inclusions of silicon carbide in moissanite from kimberlite rocks—A new find in nature. *Doklady AN SSSR* **262,** 204–206.

Mendybaev R. A., Beckett J. R., Stolper E., and Grossman L. (1998) Measurement of oxygen fugacities under reducing conditions: Non-Nernstian behavior of Y_2O_3-doped zirconia oxygen sensors. *Geochim. Cosmochim. Acta* **62,** 3131–3139.

Milton C. and Vitaliano D. B. (1984) The non-existence of moissanite, SiC (abstract). *27th Int. Geol. Congr.* **5** (Sect. 10), 107–108.

Nafziger R. H., Ulmer G. G., and Woermann E. (1971) Gaseous buffering for the control of oxygen fugacity at one atmosphere. In *Research Techniques for High Pressure and High Temperature* (ed. G. C. Ulmer), pp. 9–41. Springer-Verlag.

Narushima T., Goto T., Iguchi Y., and Hirai T. (1991) High-temperature active oxidation of chemically vapor-deposited silicon carbide in an Ar-O_2 atmosphere. *J. Am. Ceramic Soc.* **74,** 2583–2586.

Narushima T., Goto T., Yokoyama Y., Iguchi Y., and Hirai T. (1993) High-temperature active oxidation of chemically vapor-deposited silicon carbide in CO-CO_2 atmosphere. *J. Am. Ceramic Soc.* **76,** 2521–2524.

Narushima T., Goto T., Yokoyama Y., Takeuchi M., Iguchi Y., and Hirai T. (1994) Active-to-passive transition and bubble formation for high-temperature oxidation of chemically vapor-deposited silicon carbide in CO-CO_2 atmosphere. *J. Am. Ceramic Soc.* **77,** 1079–1082.

Narushima T., Goto T., Hirai T., and Iguchi Y. (1997) High-temperature oxidation of silicon carbide and silicon nitride. *Mater. Trans. JIM* **38,** 821–835.

Nicolussi G. K., Davis A. M., Pellin M. J., Lewis R. S., Clayton R. N., and Amari S. (1997) S-process zirconium in presolar silicon carbide grains. *Science* **277,** 1281–1283.

Nicolussi G. K., Pellin M. J., Lewis R. S., Davis A. M., Amari S., and Clayton R. N. (1998) Molybdenum isotopic composition of individual presolar silicon carbide grains from the Murchison meteorite. *Geochim. Cosmochim. Acta* **62,** 1093–1104.

Opila E. J. and Jacobson N. S. (1995) SiO(g) formation from SiC in mixed oxidizing-reducing gases. *Oxid. Metals* **44,** 527–544.

Opila E. J. and Hann R. E. (1997) Paralinear oxidation of CVD SiC in water vapor. *J. Am. Ceramic Soc.* **80,** 197–205.

Pultz W. W. and Hertl W. (1966) SiO_2 + SiC reaction at elevated temperatures, Part 1.—Kinetics and mechanism. *Trans. Faraday Soc.* **62,** 2499–2504.

Rosner D. E. and Allendorf H. D. (1970) High temperature kinetics of the oxidation and nitridation of pyrolytic silicon carbide in dissociated gases. *J. Phys. Chem.* **74,** 1829–1839.

Rubin A. E., Fegley B., and Brett R. (1988) Oxidation state in chondrites. In *Meteorites and the Early Solar System* (eds. J. F. Kerridge and M. S. Matthews), pp. 488–511. University of Arizona Press.

Ruzmaikina T. V. and Ip W. H. (1994) Chondrule formation in radiative shock. *Icarus* **112,** 430–447.

Schneider B., Guette A., Naslain R., Cataldi M., and Costecalde A. (1998) A theoretical and experimental approach to the active-to-passive transition in the oxidation of silicon carbide. *J. Mater. Sci.* **33,** 535–547.

Sharp C. M. and Huebner W. F. (1990) Molecular equilibrium with condensation. *Astrophys. J. Suppl. Ser.* **72,** 417–431.

Stolper E. and Paque J. M. (1986) Crystallization sequences of Ca-Al-rich inclusions from Allende: The effects of cooling rate and maximum temperature. *Geochim. Cosmochim. Acta* **50,** 1785–1806.

Tang M. and Anders E. (1988) Isotopic anomalies of Ne, Xe, and C in meteorites. II. Interstellar diamond and SiC: Carriers of exotic noble gases. *Geochim. Cosmochim. Acta* **52,** 1235–1244.

Tscharnuter W. M. and Boss A. P. (1993) Formation of the protosolar nebula. In *Protostars and Planets III* (eds. E. H. Levy and J. I. Lunine), pp. 921–938. University of Arizona Press.

Tso S. T. and Pask J. A. (1982) Reaction of fused silica with hydrogen gas. *J. Am. Ceramic Soc.* **65,** 457–460.

Turkdogan E. T., Grieveson P., and Darken L. S. (1963) Enhancement of diffusion-limited rates of vaporization of metals. *J. Phys. Chem.* **67,** 1647–1654.

Virag A., Wopenka B., Amari S., Zinner E., Anders E., and Lewis R. S. (1992) Isotopic, optical, and trace element properties of large single SiC grains from the Murchison meteorite. *Geochim. Cosmochim. Acta* **56,** 1715–1733.

Weidenschilling S. J. (1977) Aerodynamics of solid bodies in the solar nebula. *Mon. Not. R. Astron. Soc.* **180,** 57–70.

Wood J. A. and Morfill G. E. (1988) A review of solar nebula models. In *Meteorites and the Early Solar System* (eds. J. F. Kerridge and M. S. Matthews), pp. 329–347. University of Arizona Press.

Yoneda S. and Grossman L. (1995) Condensation of CaO-MgO-Al_2O_3-SiO_2 liquids from cosmic gases. *Geochim. Cosmochim. Acta* **59,** 3413–3444.

Zheng Z., Tressler R. E., and Spear K. E. (1990) Oxidation of single-crystal silicon carbide; Part 1: Experimental studies. *J. Electrochem. Soc.* **137,** 854–858.

Zinner E., Tang M., and Anders E. (1987) Large isotopic anomalies of Si, C, N and noble gases in interstellar silicon carbide from the Murray meteorite. *Nature* **330,** 730–732.